PERGAMON

Vision Research 41 (2001) 2779–2797

Vision Research

www.elsevier.com/locate/visres

Augmented rod bipolar cell function in partial receptor loss: an ERG study in P23H rhodopsin transgenic and aging normal rats

Tomas S. Aleman [a], Matthew M. LaVail [b], Rodrigo Montemayor [a], Gui-shuang Ying [a], Maureen M. Maguire [a], Alan M. Laties [a], Samuel G. Jacobson [a], Artur V. Cideciyan [a,*]

[a] *Department of Ophthalmology, Scheie Eye Institute, University of Pennsylvania, 51 North 39th Street, Philadelphia, PA 19104, USA*
[b] *Departments of Anatomy and Ophthalmology, Beckman Vision Center, University of California, San Francisco, CA, USA*

Received 30 October 2000; received in revised form 16 March 2001

Abstract

Physiological consequences of early stages of photoreceptor degeneration were examined in heterozygous P23H rhodopsin transgenic (Tg) and in aging normal Sprague–Dawley rats. Rod photoreceptor and rod bipolar (RB) cell function were estimated with maximum value and sensitivity parameters of P3 and P2 components of the electroretinogram. In both Tg and aging normal rats, the age-related rate of decline of P3 amplitude was steeper than that of the P2 amplitude. Tg rats showed greater than normal sensitivity of the rods. A new model of distal RB pathway connectivity suggested photoreceptor loss could not be the sole cause of physiological abnormalities; there was an additional increase of post-receptoral sensitivity. We propose that changes at rod-RB synapses compensate for the partial loss of rod photoreceptors in senescence and in early stages of retinal degeneration.

Keywords: Aging; Autosomal dominant retinitis pigmentosa; Electroretinogram; Reactive synaptogenesis; Rhodopsin; Rod photoreceptors; Rod bipolar cells; Sprague–Dawley albino rat

1. Introduction

Human retinopathies within the diagnostic spectrum of retinitis pigmentosa (RP) are caused by mutations in genes primarily expressed in rod photoreceptors or retinal pigment epithelial (RPE) cells (Rattner, Sun & Nathans, 1999; Clarke, Heon & McInnes, 2000a; Phelan & Bok, 2000). One of the best-studied forms of RP is caused by mutations in the *rhodopsin* (*RHO*) gene, which is expressed in rods (Dryja et al., 1990; Gal, Apfelstedt-Sylla, Janecke, & Zenner, 1997). Even though the key function of rhodopsin in phototransduction is well understood, the detailed pathophysiology of *RHO*-associated autosomal dominant RP (*RHO*-ADRP) is not known. Studies of eye-donors with *RHO*-ADRP have helped define the histopathologic characteristics of the degenerating retina (Kolb & Gouras, 1974; Tucker & Jacobson, 1988; Li, Jacobson, & Milam, 1994; Milam, Li, Cideciyan, & Jacobson, 1996; Cideciyan et al., 1998a). The end stage of disease is typified by large retinal regions devoid of photoreceptors; as expected, there is no perception of light in the corresponding areas of the patients' visual field. The earliest stages of some forms of *RHO*-ADRP, on the other hand, can have normal appearing retinal morphology; corresponding areas in the visual field are characterized by near-normal sensitivity to light and abnormally slow resensitization of rods following bright adapting lights (Jacobson, Kemp, Sung, & Nathans, 1991; Kemp, Jacobson, Roman, Sung, & Nathans, 1992; Birch, Hood, Nusinowitz, & Pepperberg, 1995; Cideciyan et al., 1998a).

What are the physiological consequences of partial loss of rods on the surviving photoreceptors and their post-synaptic targets? If one assumes retention of normal retinal circuitry among surviving neurons, an orderly relationship between number of surviving photoreceptors and overall visual dysfunction would be

* Corresponding author. Tel.: +1-215-662-9986; fax: 1-215-662-9388.
E-mail address: cideciya@mail.med.upenn.edu (A.V. Cideciyan).

0042-6989/01/$ - see front matter
PII: S0042-6989(01)00157-2

expected. However, there have been hints of changes in circuitry; if retinal circuitry is modified overall visual dysfunction may not necessarily correlate directly with photoreceptor loss. Histopathological studies in retinal regions with partial rod loss in *RHO*-ADRP have demonstrated the existence of abnormal neurites extending from surviving rod synapses into the inner retina (Li, Kljavin, & Milam, 1995; Milam et al., 1996; Fariss, Li, & Milam, 2000). These findings are not unlike reactive synaptic changes observed in the neurodegenerative diseases of the central nervous system, where partially deafferentated neurons can modify their connectivity to pre-synaptic neurons (Cotman & Nieto-Sampedro, 1984). Theoretically, reactive synaptic changes can either compensate for the primary pathology or exacerbate it (Cowan, 1970; Weller & Kaas, 1989; Sherrard & Bower, 1998). In the retina for example, observation of a disproportionate loss of inner retinal function in some patients with presumed primary photoreceptor degeneration (Hood & Greenstein, 1990; Cideciyan & Jacobson, 1993) could be taken as evidence of remodeling at surviving photoreceptor synapses amplifying the dysfunction due to the primary disease. To the knowledge of the authors, there have not been examples of compensatory reactive synaptic changes in hereditary human retinal degenerations.

Animal models of human disease help elucidate pathophysiological mechanisms and allow attempts of various experimental therapies. Naturally occurring animal models of *RHO*-ADRP do not exist, but rodent and porcine models of *RHO*-ADRP have been genetically engineered (for example, Olsson et al., 1992; Naash, Hollyfield, al-Ubaidi, & Baehr, 1993; Chang, Hao, & Wong, 1993; Portera-Cailliau, Sung, Nathans, & Adler, 1994; Chen, Makino, Peachey, Baylor, & Simon, 1995; Li, Snyder, Olsson, & Dryja, 1996; Steinberg et al., 1996; Petters et al., 1997; Humphries et al., 1997; Li et al., 1998a). Most of the animal studies have concentrated on different aspects of the primary pathology of the photoreceptors; however, there has also been evidence for synaptic abnormalities. For example, surviving rods in Pro347Leu *RHO* transgenic pigs lack synaptic vesicles and ribbons (Li et al., 1998b; Blackmon et al., 2000). Electrophysiological studies in these pigs have shown a lack of transmission of rod photoreceptor signals to rod bipolar (RB) cells and provided a possible physiological correlate to this histopathologic observation (Banin et al., 1999). The same transgenic pigs also show plasticity of rod photoreceptor synapses as documented by neurite sprouting (Li et al., 1998b) and ectopic synaptogenesis between cones and RB cells (Peng, Hao, Petters, & Wong, 2000). The observed abnormalities in cone-driven post-receptoral function (Banin et al., 1999) may be associated with these cone retinal circuitry abnormalities but further studies are necessary.

Another animal model of *RHO*-ADRP is the transgenic (Tg) rat with a proline-23 to histidine (Pro23His) *RHO* mutation (Steinberg et al., 1996; Lewin et al., 1998; LaVail et al., 2000; Machida et al., 2000). Electrophysiological results in these animals point to a relative retention of signals originating from the post-receptoral cells driven by rods (Cideciyan et al., 1999a; Machida et al. 2000). The basis of this phenomenon is not known but two possible explanations, buffering by wide receptive fields of bipolar cells and modification of synapses, have been suggested (Machida et al., 2000). In order to better understand the pathophysiology, we investigated the natural history of receptoral and postreceptoral function in the Tg rats. We also studied the maturation and normal aging of retinal function in control rats considering very little is known about receptoral and postreceptoral function between the age of 1 month and adulthood (Fulton, Hansen, & Findl, 1995). There was a progressive reduction of receptoral and postreceptoral signal amplitude both in Tg and control rats with age; the reduction in Tg rats was more extensive than the normal rats. Both in Tg and aging normal rats, the amplitude of signals originating from rod bipolar (RB) cells were better preserved than signals originating from rod photoreceptors. To test the hypothesis that buffering by wide receptive fields was the basis of the retained RB cell function in Tg and aging normal rats, we developed a model of connectivity and signaling at the distal portion of the RB cell pathway. The model results were not consistent with this hypothesis.

We propose that increased sensitivity of RB cells due to synaptic remodeling following partial loss of rod photoreceptors forms the basis of the observed pathophysiology in Tg and aging normal rats. So-called reactive synaptogenesis, if confirmed by other experiments, could form an effective functional reserve at the first synapse of the visual system and play an important role in hereditary retinal degenerations and aging by delaying symptoms and maintaining visual function that would otherwise decline more rapidly. A catastrophic loss of function would be predicted to occur at the end stages of photoreceptor degeneration when compensation is no longer possible.

2. Methods

2.1. Animals

Normal albino Sprague–Dawley (SD) rats ($n = 12$) and heterozygous transgenic (Tg) rats ($n = 10$), which were the progeny of matings between SD rats and homozygous transgenic rats with P23H mutation (line TgN(P23H)3, also on SD background), were used in the current work. Transgenic rats were produced by Chrysalis DNX Transgenic Sciences, Princeton, NJ and

developed in the laboratory of one of us (MML). All rats were raised from birth in 12-h-on-12-h-off cycles of dim (<3 lux) incandescent light. Recordings were made at ages of 1, 2, 3, 4, 5, 7, 13, and 18 months; both groups of animals were investigated during the same period and with the same equipment. The number of rats used at each age varied from 3 to 7 with two exceptions: one normal rat was available at 7 months and two normal rats were available at 18 months. The studies were conducted in accordance with the ARVO Statement for the Use of Animals in Ophthalmic and Vision Research and Institutional Guidelines.

2.2. Electroretinogram (ERG)

Full field ERGs were recorded from one dilated eye of each animal using a custom-built ganzfeld, a computer-based system (EPIC-XL, LKC Technologies, Gaithersburg, MD) and specially-made contact lens electrodes (Hansen Ophthalmics, Iowa City, IA). The signals were amplified (band-pass; -3 dB cutoff at 0.3 and 1500 Hz) and digitized with an 12-bit analog-to-digital converter at 2 or 3.33 kHz (depending on stimulus strength). Light levels were measured with a calibrated photometer (IL1700, International Light, Newburyport, MA). Animals were anesthetized with intramuscular injection of a mixture of ketamine HCl (75 mg kg^{-1}) and xylazine (5 mg kg^{-1}) under dim red lights. All ERG responses were obtained within 30 min of the anesthetic injection in order to avoid reduction in retinal illuminance secondary to anesthesia-induced cataracts (Calderone, Grimes, & Shalev, 1986; Nusinowitz, Azimi, & Heckenlively, 2000). Corneas were anesthetized with proparacaine (HCl) and pupils dilated with tropicamide (1%) and phenylephrine (2.5%).

Medium energy (10 μs duration) and high energy (1 ms duration) flash stimulators with unattenuated luminances of 0.8 and 3.6 log scot-cd s m^{-2}, respectively, were used in the current work (Cideciyan & Jacobson, 1996; Banin et al., 1999). Neutral density (Wratten 96, Kodak, Rochester, NY) and blue (Wratten 47A) filters attenuated and spectrally shaped the flashes to produce ten standard blue stimuli in the range of -4.2 to $+2.2$ log scot-cd s m^{-2}. Dark-adapted (>12 h) ERGs were obtained with blue stimuli increasing from -4.2 to -1.2 log scot-cd s m^{-2} (see waveforms labeled I–VIII in Fig. 1A) in 0.3–0.5 log unit steps; 2–8 responses were averaged with interstimulus intervals increasing from 2 to 30 s. After a 1 min wait, a single flash (non-averaged) response was evoked with a $+0.6$ log scot-cd s m^{-2} blue stimulus (Fig. 1A, waveform IX). After an additional ca. 5 min wait, a single flash response was evoked with a $+2.2$ log scot-cd s m^{-2} blue stimulus (Fig. 1A, waveform X).

In order to estimate the cone contribution in the dark-adapted ERG waveforms, pilot studies were performed under light-adapted (30 cd m^{-2}, white) conditions (not illustrated in the current work). The $+2.2$ log scot-cd s m^{-2} blue stimulus evoked ERG b-waves of >100 μV amplitude but -1.2 log scot-cd s m^{-2} blue stimulus did not evoke detectable responses under light adapted conditions. This finding was consistent with published cone ERG thresholds of approximately -1 log cd s m^{-2} in rats (Sugawara, Sieving, & Bush, 2000) and mice (Toda, Bush, Humphries, & Sieving, 1999); light-adapted ERGs were not further pursued. Cone-derived component of the $+0.6$ log scot-cd s m^{-2} blue stimulus was ignored since only the leading edge of this response was used in the current work and the dominant ($>95\%$, see below) contributor to the leading edge was rod-derived. Cone-derived ERG component of the maximal stimulus ($+2.2$ log scot-cd s m^{-2} blue) was determined, however, in each experiment with a paired-flash procedure (Birch et al., 1995; Pepperberg, Birch, Hofmann, & Hood, 1996; Cideciyan et al., 1998b; Pepperberg, Birch, & Hood, 2000). Our procedure was an abbreviated version consisting of a single conditioning flash strength (white 3.6 log scot-cd s m^{-2}) and a single interflash interval (30 s). This interval was chosen to be longer than the expected time for full recovery of the cone component (Lyubarsky, Falsini, Pennesi, Valentini, & Pugh, 1999; Lyubarsky, Chen, Simon, & Pugh, 2000) and shorter than the initiation of rod recovery (>180 s) determined in pilot studies (data not shown).

2.3. Estimated retinal illuminance

An estimate of retinal illuminance resulting from viewing a homogenous ganzfeld allows comparison between non-invasive ERG results and single cell recordings. For the current work, we will assume a flash of 1 scot-cd s m^{-2} produces ca. 2000 isomerizations per rod in normal adult albino rats raised under dim cyclic light conditions. This estimate is similar to some previous estimates in pigmented (Bush, Hawks, & Sieving, 1995) and albino (Naarendorp & Williams, 1999) rats. Similar dark-adapted thresholds in albino and pigmented rats (Green, Herreros de Tejada, & Glover, 1991) suggest that at least under pupillary dilation, ocular pigmentation does not significantly affect retinal illuminance. In adult mice, retinal illuminance resulting from a 1 scot-cd s m^{-2} luminance has been estimated (using different sets of assumptions) at ca. 100 (Hetling & Pepperberg, 1999), ca. 1500 (Pennesi, Lyubarsky, & Pugh, 1998) and ca. 5000 (Goto et al., 1996) isomerizations per rod. Based on geometric considerations (illuminance is proportional to pupillary area and inversely proportional to ocular axial length), retinal illuminance of the adult rat should be ca. 20% larger than the mouse when viewing the same homogeneous extended light source. Thus, our estimate in the rat falls near the middle of the range of estimates in the mouse.

2.4. Model of the activation phase of rod phototransduction: analysis of the P3 component

The leading edges (ca. 4–10 ms depending on stimulus energy) of ERG responses evoked by 0.6 and 2.2 log scot-cd s m^{-2} (8×10^3 and 300×10^3 isomerizations/rod) stimuli would be expected to represent the activity of photoreceptors (Pugh, Falsini, & Lyubarsky, 1998). Based on classical analyses (Granit, 1933) and more recent research (Hood, Shady, & Birch, 1993), this portion of ERG photoresponses has been called the P3 component. Dark-adapted P3 component is usually

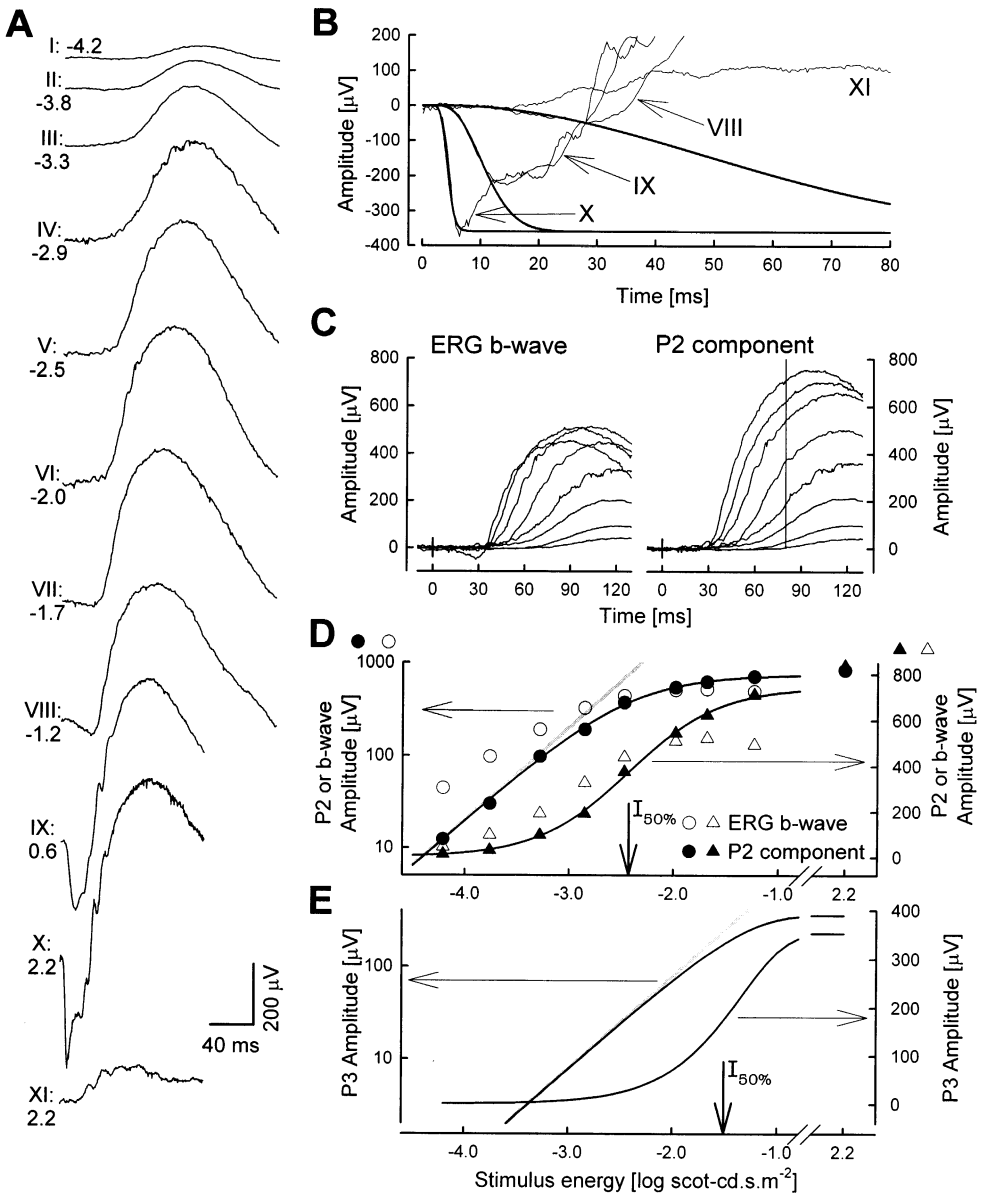

Fig. 1. Analysis of P3 and derived P2 components of the normal rat ERG. (A) Raw ERG waveforms recorded in a representative 5 month-old normal rat. Stimulus energy of each waveform (I–XI) is shown in log scot-cd s m^{-2} units. All waveforms start at the time of stimulus presentations and calibration is shown on the lower right. (B) The alternative model of phototransduction activation (thick smooth lines) was fit as an ensemble to waveforms IX and X. Extrapolation of the model parameters to the stimulus energy of waveform VIII shows the correspondence at early times between the model and the ERG a-wave. The dark-adapted cone component (XI) corresponding to the maximal stimulus response (X) shows no apparent a-wave. (C) Comparison of the initial 130 ms of raw ERG b-waves and the derived P2 components. Thin vertical line marks 80 ms time point used in the current work. (D) Luminance-response functions of traditionally measured ERG b-wave amplitudes (unfilled symbols) and the derived P2 component at 80 ms (filled symbols). Data are displayed on two ordinates for clarity: logarithmic scale (circles, left) enhances the smaller amplitude region and the linear scale (triangles, right) enhances the larger amplitude region. Fit of a simple hyperbolic function (black lines) as well as the region of linearity (gray diagonal line) are shown. $I_{50\%}$ refers to the stimulus energy that evokes 50% of saturated amplitude. Note the ca.3 log unit break in the abscissa to allow the display of the amplitude at maximal stimulus for reference. (E) Luminance-response function of the P3 component at 80 ms. Logarithmic and linear ordinates similar to panel D.

dominated by the rod photoreceptor activity but varying amounts of cone activity can contribute depending on the species under consideration (Cideciyan et al., 1999b). In mice, cone contribution to the P3 component is minuscule (Lyubarsky et al., 1999) and rats would be expected to have even smaller cone contribution (Deegan & Jacobs, 1993; Williams, Webbers, Giordano, & Henderson, 1998). Analysis of the leading edges of the dark-adapted cone component in the rat showed that cones contribute less than 5% of the amplitude of the rod P3 component at 1 month of age (data not shown); at later ages, a distinct cone component could not be unequivocally demonstrated within the noise of the recordings (waveform XI, Fig. 1A and B).

The rat P3 component was analyzed using an alternative model of rod phototransduction activation defined as:

$$\mathrm{P3}(I,t) = \mathrm{P3}_{\max}\left(1 - \exp\left\{-\frac{1}{2} I\sigma\left[(\varepsilon^2 - 6\varepsilon\tau + 12\tau^2) - \mathrm{e}^{\frac{-\varepsilon}{\tau}}(\varepsilon^2 - 6\varepsilon\tau + 12\tau^2)\right]\right\}\right) * \mathrm{e}^{\frac{-\varepsilon}{\tau_{\mathrm{m}}}} \quad (1)$$

where $\mathrm{P3}(I, t)$ is the leading edge of the corneally measured potential in μV; I is the retinal illuminance of the stimulus in scot-td s; t is the time after stimulus onset in seconds; $\mathrm{P3}_{\max}$ is the maximum amplitude in μV; σ is the sensitivity in scot-cd^{-1} m^2 s^{-3}; ε is time, t, delayed by a constant ($\varepsilon = t - \delta$); τ is the time constant of three first-order decays presumed to correspond to three dominant photoactivation reactions; τ_{m} is the capacitive time constant of the photoreceptor membrane; and, * represents the convolution operation (Cideciyan & Jacobson, 1996; Cideciyan, 2000). This alternative model considers the earliest stages of biochemical reactions as a cascade of three dominant first-order reactions instead of a simple time delay used in the delayed Gaussian model (Lamb & Pugh, 1992; Pugh & Lamb, 1993). The alternative model has been shown to describe photoresponse activation kinetics simultaneously over a large range of stimulus intensities in several mammalian species including man, monkey, pig and rat (Cideciyan et al., 1999b) and in retinal degenerative diseases of man (Cideciyan et al., 1998a; Cideciyan, 2000), pig (Banin et al., 1999) and mice (Van Hooser et al., 2000). The alternative model of rod phototransduction was fit simultaneously to the P3 components evoked with $+0.6$ and $+2.2$ log scot-cd s m^{-2} stimuli (Fig. 1B). Only the two variables of the model, saturated amplitude ($\mathrm{P3}_{\max}$) and sensitivity (σ), were allowed to vary; other parameters (δ, τ, τ_{m}) were unchanged from the original description of the model in man (Cideciyan & Jacobson, 1996) under the assumption of stereotypy of phototransduction activation in mammalian rods (Pugh & Lamb, 1993).

$\mathrm{P3}_{\max}$ is believed to be proportional to the total number of cyclic nucleotide gated (CNG) channels on rod outer segment (ROS) plasma membranes open in the dark across the retina (Breton, Schueller, Lamb, & Pugh, 1994; Hood & Birch, 1994). Assuming CNG channel density does not change secondary to the outer retinal degeneration, the fraction of Tg rat $\mathrm{P3}_{\max}$ compared to the age-matched normal rat value provides a quantitative and non-invasive measure of the total extent of photoreceptor degeneration across the retina. Assuming that all functioning rods activate stereotypically with light in normal and Tg rats, the σ parameter provides a quantitative (and absolute) measure of phototransduction amplification gain (Pugh & Lamb, 1993).

2.5. Derivation and analysis of the P2 component

During the last decade, there has been increasing evidence that the leading edge of the ERG b-wave originates primarily from the activity of RB cells (e.g. Gurevich & Slaughter, 1993; Xu & Karwoski, 1994; Robson & Frishman, 1995; Hood & Birch, 1996; Karwoski & Xu, 1999; Lei & Perlman, 1999; Shiells & Falk, 1999; Kofuji et al., 2000). When isolated from potentials believed to originate in more distal or more proximal retinal cells, the ERG b-wave is called the P2 component (Hood & Birch, 1992). We derived the P2 component of the rat ERG at low illumination (-4.2 to -1.2 log scot-cd s m^{-2}; ca. 0.1–100 isomerization/rod) by subtracting the P3 component estimated from ERG data at higher illumination and extrapolated to lower illumination. In the current work, we will use the term 'P2' to refer to the computationally derived P2 component of the ERG. Fig. 1B shows a representative example where the P3 component is estimated from the leading edges of responses evoked by high illumination (waveforms IX and X) and applied to a response evoked by low illumination (waveform VIII). The extrapolated P3 component appears to describe the a-wave component of this low intensity response.

Comparison of the traditionally-measured ERG b-waves and the P2 component (Fig. 1C) shows the larger amplitudes achieved in the latter. ERG b-wave amplitudes as a function of luminance have been parameterized with models to describe their sensitivity to light in rodents (e.g. Cone, 1963; Green et al., 1991; Pugh et al., 1998). Based on recent studies on pharmacologically isolated bipolar cell responses (Robson & Frishman, 1995, 1999), we determined the light dependence of the P2 component by modeling the amplitude as a function of luminance at a fixed time. In order to choose an

appropriate value for this fixed time, we took into account the following competing considerations: (1) as early as possible, to allow the use of the P3 model which does not include effects of deactivation reactions (must be earlier than ca. 100 ms in mice; Pugh & Lamb, 1993; Chen et al., 1995, 1999; Hetling & Pepperberg, 1999); (2) as early as possible, to avoid the trailing edge of the P2 responses (must be earlier than ca. 90 ms in the current set of experiments); (3) as late as possible, to allow detectable responses evoked by the weakest stimulus used in these studies (must be later than ca. 80 ms in the current set of experiments). Based on these considerations we choose 80 ms (Fig. 1C, right panel). It is important to point out that when extrapolating the P3 component measured at ca. 5–15 ms to ca. 80 ms, we are implicitly assuming the time-invariance of the parameters describing this component. There is recent evidence that the amplification factor accelerates with time in mice (Hetling & Pepperberg, 1999); a plausible biochemical model has been hypothesized to underlie this acceleration (Pepperberg, 1998). The extent of this amplification acceleration in normal or Tg rats is currently not known and was not pursued in the current work.

P2 amplitude at 80 ms was fit with a simple hyperbolic function:

$$P2_{80}(I) = P2_{max}\left\{\frac{I}{I+K}\right\} \quad (2)$$

where $P2_{80}$ (I) is the P2 amplitude in μV measured at 80 ms; $P2_{max}$ is the saturated amplitude; I is the light stimulus energy in scot-cd s m^{-2}; and K is the semisaturation constant in scot-cd s m^{-2}. This function described the data well over low (Fig. 1D, logarithmic scale) and high (Fig. 1D, linear scale) amplitudes. Traditionally measured (peak-to-peak) ERG b-wave amplitudes had a shallower rise and a lower saturated amplitude (Fig. 1D). Comparison of the amplitude with a 3 log unit higher stimulus (waveform X, Fig. 1A and D) after subtraction of the cone component (waveform XI) and P3 component suggested that the saturated amplitude estimate of the P2 component was consistent across a large intensity range. Traditionally measured ERG b-wave amplitudes showed two saturation limbs with different plateaux as described in mice (Toda et al., 1999).

The fit of the simple hyperbolic function to the P2 amplitudes has the important consequence of linearity at low illumination levels (Fig. 1D, gray diagonal line). Previously, this property has been taken as evidence of a dominant RB component within the response (Robson & Frishman, 1995; Hood & Birch, 1996) based on observations of small-signal linearity in dogfish on-bipolar recordings (Ashmore & Falk, 1980). More recently, light evoked responses of mouse (Berntson & Taylor, 2000) and rat (Euler & Masland, 2000) RB cells have been fit with equations that closely approximate the simple hyperbolic function. The scotopic threshold response (STR) component of the ERG, that has been demonstrated to affect small signal linearity in the cat (Robson & Frishman, 1995), was not apparent in our recordings. It is possible that protocol differences abolished the rat STR (Bush et al., 1995; Frishman & Sieving, 1995; Hood & Birch, 1996) or the STR component was negligible at the 80 ms time chosen. Therefore, for the purposes of the current work, we will assume that electrical activity of RB cells are the dominant contributors of the P2 component, as recorded and analyzed here.

2.6. Measures of sensitivity

In order to compare sensitivities of the P3 and P2 components, we choose a consistent measure: reciprocal of the stimulus energy that evokes 50% of the saturated amplitude at 80 ms time chosen ($I_{50\%}$ shown in Fig. 1D and E). For the P3 model (Eq. (1)), the effect of the convolution term is negligible at times that are long compared to the time constants involved and thus the sensitivity for the P3 component of the ERG at 80 ms can be well approximated with:

$$P3_{sens} = \sigma\left[\frac{(\varepsilon^2 - 6\varepsilon\tau + 12\tau^2)}{2\cdot\ln(2)}\right] \quad (3)$$

where σ, ε and τ have been previously defined in Eq. (1). At the fixed time ($t = 80$ ms) considered in the current work, the term in square brackets evaluates to 0.0042 s^2. In turn, the sensitivity for the P2 component is defined as:

$$P2_{sens} = \frac{1}{K} \quad (4)$$

where K is the semisaturation intensity of the hyperbolic function (see Eq. (2)) fit to the P2 component amplitude at 80 ms. Both measures of sensitivity use inverse light energy units ((scot-cd s m^{-2})$^{-1}$ or equivalently, scot-cd^{-1} s^{-1} m^2). An increase in light sensitivity shifts the appropriate saturation curve to the left (Fig. 1D and E).

2.7. Models of natural history

The dominant tendency for amplitude parameters ($P2_{max}$ and $P3_{max}$) was to decrease with age over the 1 to 18 month range studied (see Section 3 below). The age-dependency of these parameters appeared nonlinear. An exponential function was considered based on progression of human RP (Berson, Sandberg, Rosner, Birch, & Hanson, 1985; Massof & Finkelstein, 1987; Birch, Anderson, & Fish, 1999) and a recent hypothesis on the decline of cell numbers in a wide range of neurodegenerative conditions (Clarke et al., 2000b). A

single exponential did not account for the apparent faster rate of change at early ages and slower rate of change at later ages. Therefore, we used a double exponential to describe the age-dependence of the amplitude parameters. The specific equation chosen was:

$$P2/3_{max}(age) = A\left(2e^{\frac{-age}{\tau_1}} + e^{\frac{-age}{\tau_2}}\right) \quad (5a)$$

where $P2/3_{max}$ refers to $P2_{max}$ or $P3_{max}$; age is in months; A is a scaling parameter in μV; and, τ_1 and τ_2 are the time constants in months for the hypothesized fast/early and slow/late components, respectively.

The sensitivity parameters ($P2_{sens}$ and $P3_{sens}$) showed a tendency to increase with age (see Section 3 below). Under the parsimonious assumption that the age-dependency of semisaturation constants ($I_{50\%}$) have the same functional form as Eq. (5a), we chose the reciprocal of Eq. (5a) to describe the natural history of sensitivity parameters. The equation was:

$$P2/3_{sens}(age) = \frac{S}{\left(2e^{-\frac{age}{\tau_1}} + e^{-\frac{age}{\tau_2}}\right)} \quad (5b)$$

where $P2/3_{sens}$ refers to $P2_{sens}$ or $P3_{sens}$; age is in months; S is a scaling parameter in scot-cd^{-1} s^{-1} m^2; and, τ_1 and τ_2 are the time constants in months for the hypothesized fast/early and slow/late components, respectively. Models of natural history were fit to the raw data by minimizing the sum of squared error terms using a simplex algorithm (Matlab Version 4.2; The Mathworks, Natick, MA).

2.8. Statistical analyses

Variation of the four measured parameters ($P3_{max}$, $P2_{max}$, $P3_{sens}$, and $P2_{sens}$) was studied as a function of animal group (Tg or normal) and age using a mixed linear model with repeated measurements (Littell, Milliken, Stroup, & Wolfinger, 1996). To avoid the assumption of a linear effect of age on the measured parameter, age was initially treated as a categorical variable. Results are presented only for a main effects model with group and age as covariates since no statistically significant interactions were found for any of the parameters between group and age (not shown).

In an effort to quantify the statistical significance of the rate of retinal functional loss due to degeneration, data determined to have significant age effects were analyzed *post-hoc* with linear regression using age as a continuous covariate. For this analysis, parameter values were logarithmically transformed and values originating at ages of 1 and 2 months were disregarded (under the assumption that eye growth is a dominant factor at these early times). The slope coefficients of the regression line and their 95% confidence intervals were estimated for each of the four parameters with age. Confidence intervals were used to determine difference of slopes from zero. The differences of slope coefficients between normal and Tg rats were tested based on the interaction between age and group from the mixed linear model. The differences in slope coefficients between $P2_{max}$ and $P3_{max}$, between $P2_{sens}$ and $P3_{sens}$ for a given group were tested based on the interaction between age and parameter indicator. Slope coefficients of logarithmically transformed data are presented as time constants for easier comparison with the results of non-linear regression analysis.

The magnitude of the derived parameters (the ratio of measured to predicted sensitivity in normal or Tg rats) was compared to the theoretically expected value of 1. This overall comparison was achieved by t-test taking into account repeated measurements. All analyses were performed with PC SAS (ver. 8.01, SAS Institute, Cary, NC). Data are presented with mean value and $\pm$95% confidence intervals.

3. Results

3.1. Maturation and aging of retinal function in normal rats

We studied normal rats from 1 to 18 months of age to establish ERG parameters as a function of normal maturation and aging, and used these parameters comparatively to interpret the functional consequences of retinal degeneration in Tg rats. Representative ERG results are presented at the ages of 2 and 13 months (Fig. 2). ERGs recorded from the same normal rat 11 months apart showed a large reduction of $P3_{max}$ (Fig. 2B and E left panels) but little change in $P2_{max}$ (Fig. 2C and F left panels). Summary data were orderly and confirmed this difference between natural histories of $P3_{max}$ and $P2_{max}$ parameters (Fig. 3A). The $P3_{max}$ parameter at 13 months (338 ± 38 μV) was reduced to 63% of the value at 2 months (538 ± 66 μV); the $P2_{max}$ parameter at 13 months (779 ± 145 μV), on the other hand, was 83% of the value at 2 months (937 ± 154 μV). Both parameters appeared to decline initially fast and in parallel, and later slow and diverging (Fig. 3A). Both parameters showed statistically significant age effects (Table 1). Nonlinear regression analysis resulted in τ_1 of ca. 0.5 months for both parameters, and τ_2 of 29 and 67 months for $P3_{max}$ and $P2_{max}$, respectively (Table 2).

Similarity of the faster rate of decline of $P2_{max}$ and $P3_{max}$ most likely represents early changes of the electrical properties of the globe as the rat eye grows (for example, Katz & Robison, 1986); developmental apoptosis has mostly ended by the third post-natal week in rodents (for example, Young, 1984) and thus is not expected to contribute. The slower phase of decline

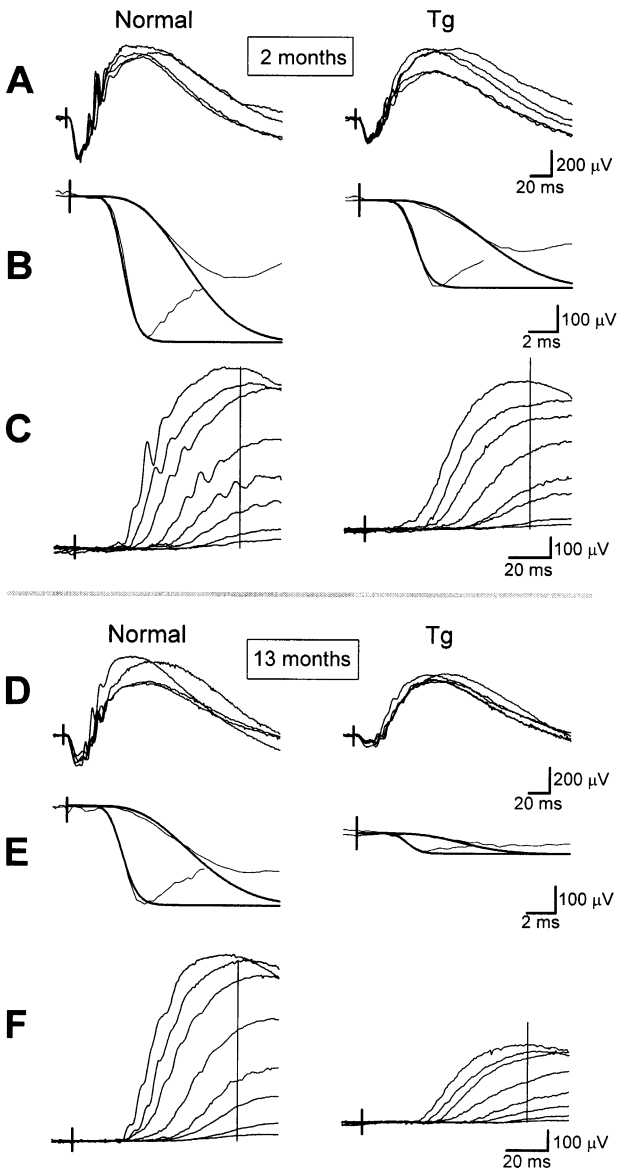

Fig. 2. Representative ERGs of normal (left panels) and transgenic (Tg, right panels) rats at two months (A, B, C) and 13 months (D, E, F) of age. (A, D) Raw ERG waveforms evoked by 0.6 log scot-cd.s.m^{-2} stimulus. Experimental variability is demonstrated in different normal ($n=4$) and Tg ($n=5$) rats. (B, E) Alternative model of phototransduction activation (thick smooth lines) fit as an ensemble to the leading edges of ERGs (thin noisy lines) evoked by 2.2 and 0.6 log scot-cd s m^{-2} stimuli. Normal $P3_{max}=554$ μV, $P3_{sens}=78$ scot-cd^{-1} s^{-1} m^2 (panel C), $P3_{max}=375$ μV, $P3_{sens}=64$ scot-cd^{-1} s^{-1} m^2 (panel F). Transgenic $P3_{max}=332$ μV, $P3_{sens}=58$ scot-cd^{-1} s^{-1} m^2 (panel C), $P3_{max}=76$ μV, $P3_{sens}=90$ scot-cd^{-1} s^{-1} m^2 (panel F). (C, F) The derived P2 component (thin noisy lines) evoked by -4.2 to -1.2 log scot-cd s m^{-2} stimuli, and the 80 ms time point (long vertical lines) used in the current work. Normal $P2_{max}=927$ μV, $P2_{sens}=389$ scot-cd^{-1} s^{-1} m^2 (panel C), $P2_{max}=988$ μV, $P2_{sens}=372$ scot-cd^{-1} s^{-1} m^2 (panel F). Transgenic $P2_{max}=744$ μV, $P2_{sens}=295$ scot-cd^{-1} s^{-1} m^2 (panel C), $P2_{max}=418$ μV, $P2_{sens}=275$ scot-cd^{-1} s^{-1} m^2 (panel F). Data from the same pair of representative animals are shown in panels B, C, E, F. Short vertical lines early in each trace represent the flash stimulus.

may likely represent rod degeneration due to aging (Shinowara, London, & Rapoport, 1982; Katz & Robison, 1986; Organisciak et al., 1998). The later phase of $P2_{max}$ decline was not as steep as that of $P3_{max}$ decline, and the difference was significant (Table 2). Furthermore, the rate of $P2_{max}$ decline appeared to slow between 2 and 3 months, whereas that of $P3_{max}$ decline slowed between 3 and 4 months (Fig. 3A). These diverging declines pointed at a mechanism causing progressive retention of $P2_{max}$ from the age of 3 months onwards, which is better demonstrated by the ratio of $P2_{max}$ to $P3_{max}$ (similar to the traditional ERG parameter of b- to a-wave ratio). This ratio was ca. 1.8 for the first 2 months and increased to ca. 2.5 by 18 months of age (Fig. 3B).

$P3_{sens}$ parameter showed an initial increase from 32.6 ($\pm$7.4) scot-cd^{-1} s^{-1} m^2 at 1 month to 61.9 ($\pm$11.1) scot-cd^{-1} s^{-1} m^2 at 2 months; there was no apparent orderly age trend at later ages (Fig. 3C). The overall age effect was statistically significant (Table 1). Nonlinear regression estimates showed a τ_1 of 0.47 months; τ_2 was a very large number (Table 2). Consistent with these results, the later phase slope was not significantly different than zero (Table 2). The age invariance of $P3_{sens}$ suggests that large losses in $P3_{max}$ do not affect the rod transduction activation in aging rats. Further support for the retention of retinal sensitivity came from analyzing the P2 component. $P2_{sens}$ was $\sim$5 times greater than $P3_{sens}$ (Fig. 3C). The natural history of the $P2_{sens}$ parameter appeared to be approximately the inverse of $P2_{max}$ variation; $P2_{sens}$ increased from 145.9 ($\pm$41.1) scot-cd^{-1} s^{-1} m^2 at 1 month to 310.8 ($\pm$39.5) scot-cd^{-1} s^{-1} m^2 at 18 months. There was a significant age effect (Table 1). Nonlinear regression estimates showed a τ_1 of 0.57 months and a τ_2 of 54 months (Table 2). Later phase slope of the $P2_{sens}$ was significantly different than zero suggesting an age-related increase in sensitivity (Table 2).

A relative retention of $P2_{max}$ whilst declining $P3_{max}$ would not be surprising under the 'local dropout' or 'diffuse loss' model of ERG signaling (Hood & Birch, 1992; Hood, Shady, & Birch, 1994) where the convergence of presynaptic rod signals to RB cells has a protective effect on RB cell function. This model would predict a *decrease* of $P2_{sens}$ in approximate proportion to the decrease in $P3_{max}$; current results showing a progressive *increase* in $P2_{sens}$ were unexpected.

3.2. Supernormal rod sensitivity and retention of RB cell function in Tg rats

The most immediately recognizable feature of a typical Tg rat ERG was a disproportionate b- to a-wave ratio (Fig. 2A and D). ERGs recorded from a representative Tg rat (Fig. 2B, C, E, and F right panels) show a much larger reduction of $P3_{max}$ (from 332 to 76 μV;

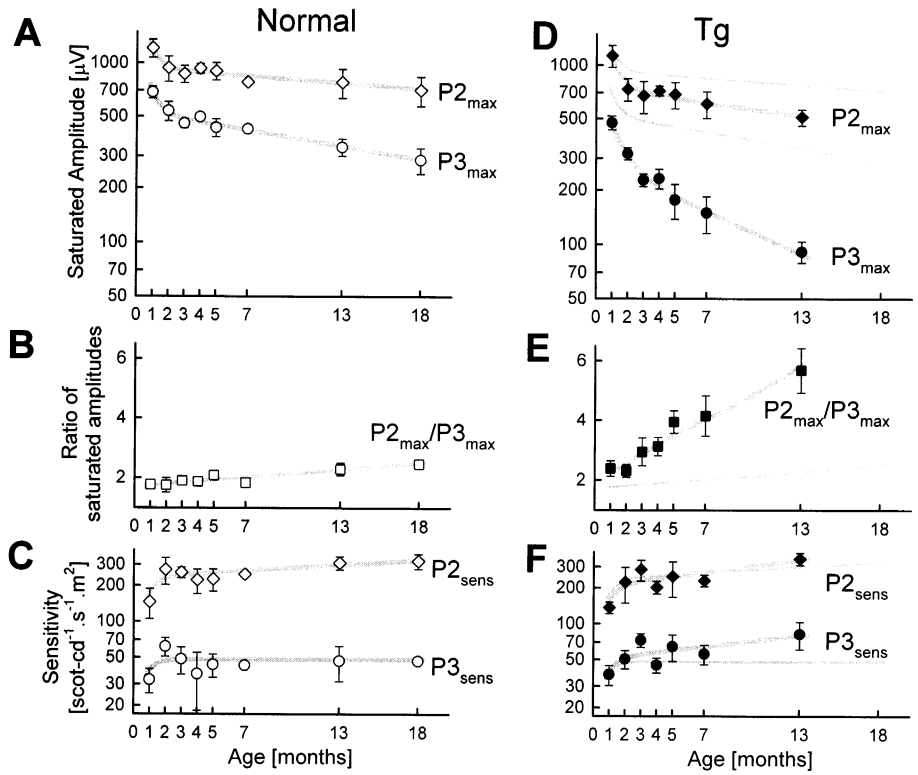

Fig. 3. Natural history of rod photoreceptor and postreceptoral function in normal and transgenic (Tg) rats. Saturated amplitudes of P2 and P3 components of the dark-adapted ERG (A, D), the ratio of the saturated amplitude of P2 component to P3 component (B, E), and sensitivity of the P2 and P3 components (C, F) are shown as a function of age. ERGs were not detectable at 18 months in Tg animals and are thus not shown. All error bars represent 95% confidence intervals. There was only one normal rat recording at 7 months thus no error bars shown. Gray lines represent double-exponential model of age-dependence fit to the data. Thin gray lines in right panels duplicate the thick gray lines of left panels for reference.

ca. 4-fold) than $P2_{max}$ (from 744 to 418 μV; ca. 1.8-fold) over the 11 month period. This Tg rat ERG feature was analyzed further by considering the natural history of the ERG parameters from 1 to 13 months of age. Summary data showed orderly progression (Fig. 3D–F). $P3_{max}$ of Tg rats was smaller than normal rats at 1 month (475 ± 42 μV) and at all subsequent ages (Fig. 3D); results from the two groups of rats were significantly different (Table 1). This was not surprising considering the line of Tg rats used in the current study are a well-accepted model of slow photoreceptor degeneration (Lewin et al., 1998; Machida et al., 2000; LaVail et al., 2000). Nonlinear regression analysis resulted in a τ_1 of 0.99 months and a τ_2 of 11 months (Table 2). Later phase of $P3_{max}$ decline in Tg rats was 2–3 times faster than normal rats (Fig. 3D); the difference between the two groups of rats was statistically significant (Table 2). Mean $P2_{max}$ of Tg rats were smaller than normal rats at all ages (Fig. 3D) and the two groups were significantly different (Table 1). Estimates for τ_1 and τ_2 were 0.71 and 35 months, respectively (Table 2). Later phase of $P2_{max}$ decline of Tg rats was different than the $P3_{max}$ decline of Tg rats but not different than the $P2_{max}$ decline of normal rats (Table 2). The divergence of $P2_{max}$ and $P3_{max}$ amplitudes in Tg rats was well demonstrated by their ratio which was ca. 2.3 for the first 2 months and progressively increased to ca. 5.7 by 13 months of age (Fig. 3E). Consistent with previous observations (Cideciyan et al., 1999a; Machida et al., 2000), Tg rat ERGs provided evidence for a retention of RB cell function qualitatively similar to that seen in normal rats but much exaggerated in extent.

It is useful to note that the amplitudes (measured at 80 ms) of the dark-adapted cone-isolated ERG b-wave of Tg rats were not different than normal rats between 1 and 7 months (for example at 3 months, normal = 138 ± 21 μV and Tg = 117 ± 17 μV); at 13 months, amplitudes of Tg rats (76 ± 18 μV) were significantly smaller than normal rats (137 ± 21 μV). At 18 months of age, the b-wave of the cone ERG and P3 and P2

Table 1
The effects (*P*-values) of group and age on the four measured parameters

Main effect model	$P3_{max}$	$P3_{sens}$	$P2_{max}$	$P2_{sens}$
Group	<0.0001	0.0077	<0.0001	0.87
Age	<0.0001	0.0035	<0.0001	<0.0001

Table 2
Estimates of natural history

	Normal				Tg				P-value[c]
	A or S[a]	τ_1[a]	τ_2[a]	$\tau_{2'}$[b]	A or S[a]	τ_1[a]	τ_2[a]	$\tau_{2'}$[b]	
$P2_{max}$	938	0.53	67	59**	748	0.71	35	31**	0.16
$P3_{max}$	534	0.55	29	29** $P=0.04$[d]	287	0.99	11	11** $P<0.001$[d]	<0.0001
$P2_{sens}$	234	0.57	54	41**	203	0.57	25	26**	0.34
$P3_{sens}$	48	0.47	10^{12}	128 $P=0.35$[e]	50	0.56	28	34 $P=0.63$[e]	0.34

[a] Non-linear regression estimates from data at all ages using Eq. (5a) for $P2_{max}$ and $P3_{max}$ and Eq. (5b) for $P2_{sens}$ and $P3_{sens}$.
[b] Linear regression estimates from logarithmically transformed data at ages ≥ 3 months. Slopes have been transformed into time constants ($\tau_{2'}$) for comparability to non-linear regression estimate (τ_2).
[c] P-value for the test of $\tau_{2'}$ difference between normal and Tg groups.
[d] P-value for the test of $\tau_{2'}$ difference between $P2_{max}$ and $P3_{max}$.
[e] P-value for the test of $\tau_{2'}$ difference between $P2_{sens}$ and $P3_{sens}$.
** Slope significantly ($P=0.05$) different than zero (i.e. $\tau_{2'}$ significantly different than $\pm\infty$).

components of the rod ERG were not detectable in Tg rats (data not shown). This suggested a relative acceleration of photoreceptor degeneration at later disease stages, which was not further explored in the current work.

The mean $P3_{sens}$ values of Tg rats were greater than those of normal rats for 6 of 7 time points tested (Fig. 3F); the difference between groups of rats was statistically significant (Table 1). Nonlinear regression analysis resulted in τ_1 of 0.56 months and τ_1 of 28 months (Table 2) but the later phase slope was not significantly different than zero (Table 2). Greater than normal sensitivity originating at the level of rods was unexpected as it has not been previously demonstrated in any form of outer retinal degeneration.

$P2_{sens}$ values of Tg rats overlapped with those of normal rats across the tested age range (Fig. 3F); two groups were not significantly different (Table 1). Natural history of this parameter could be described with a τ_1 of 0.57 months and τ_2 of 25 months (Table 2). Later phase slope was not significantly different than the normal slope (Table 2). We also determined P2 thresholds using a criterion of 35 μV at 80 ms (which approximates the 50 μV criterion for peak amplitude used by others; Green et al., 1991; Machida et al., 2000). Mean normal rat thresholds were -3.68 ($\pm$ 0.18) log scot-cd s m^{-2} at 1 month of age and fluctuated between -3.74 and -3.83 log scot-cd s m^{-2} over the age range 2–18 months. Mean Tg thresholds were higher than normal thresholds at all ages but the differences did not reach statistical significance (not shown).

Assuming observed age-related decrease of $P3_{max}$ represents rod photoreceptor degeneration, and assuming P2 component originates from activity of RB cells, the relative retention of $P2_{max}$ *and* $P2_{sens}$ is generally incompatible with the current understanding of retinal signaling and hypothetical consequences of photoreceptor loss (Hood & Birch, 1992). We derived a model of retinal circuitry in order to quantitatively estimate the extent of RB function retention in rat ERGs.

3.3. Estimate of RB sensitivity based on a model of distal RB-pathway connectivity and signaling

RB-pathway is a stereotypical circuit used by most mammals to convey rod signals to ganglion cells at scotopic (<1 isomerization per rod per integration time) light levels (Smith, Freed, & Sterling, 1986). The distal components of the RB-pathway include rods, RBs and horizontal cells; the more proximal components include amacrine cells, cone bipolars and ganglion cells. For the current model, we consider the activity of the rods and RB cells and the synaptic connections between them. RBs sum the signals from rods within their dendritic fields along both convergent and divergent pathways. We consider only patches of retina (wider than the dendritic field extent) where rods and RBs are homogeneously distributed on square grids of two parallel planes to simplify schematics. Plausible values for convergence (18:1), divergence (1:2), rod (202,500 mm^{-2}) and RB (22,500 mm^{-2}) densities are used for schematics (Fig. 4) based on rat or mouse data (for example, Cone, 1963; Boycott & Dowling, 1969; Grunert & Martin, 1991; Euler & Wassle, 1995; Jansen, Hawkins, & Sanyal, 1997; Jeon, Strettoi, & Masland, 1998; Strettoi & Pignatelli, 2000). Dendritic fields of this model have diameters of ca. 15 μm, which is somewhat smaller than anatomical estimates in the rat (Euler & Wassle, 1995).

The model assumes that pooled activities of functional rods and RBs are tracked by the P3 and P2 components of the ERG, respectively (Hood & Birch, 1992; Pugh & Lamb, 1993; Hood & Birch, 1994; Hood et al., 1994; Hood & Birch, 1996; Cideciyan et al.,

1998a; Pugh et al., 1998). The explicit purpose of the model is to estimate the expected change in the sensitivity of the functional RBs (ΔRB_{sens}; prefix Δ is used to refer to variables specified as a fraction of an appropriate control condition) given a set of experimental findings ($\Delta P3_{max}$, $\Delta P3_{sens}$, and $\Delta P2_{max}$), and a set of assumptions on the type of underlying degeneration.

Spatial distribution of hypothetical photoreceptor degenerations may be delimited by two extremes: 'diffuse' loss of rods may occur due to the action of cell-autonomous mechanisms where loss of each cell is independent of the state of neighboring cells; 'patchy' loss of rods may result from non-cell-autonomous mechanisms. We assume that a realistic representation of rod degeneration may be more intermediate in distribution with both diffuse and patchy components (Cideciyan et al., 1998a). A schematic example of such an intermediate degeneration distribution (Fig. 4B) is provided to supplement the theoretical analysis that will follow.

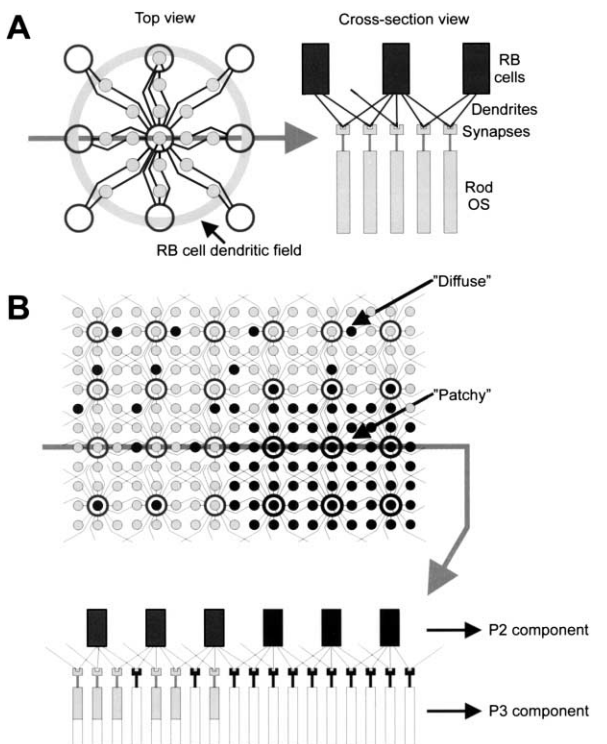

Fig. 4. Schematic diagram of the model of the distal RB cell pathway. (A) Enlarged view of RB cells (larger gray empty circles) making dendritic contact to neighboring rods (smaller gray filled circles) shown as top (left panel) and cross-sectional (right panel) views. RB cells and rods are distributed on aligned square grids of two parallel planes. Each RB cell contacts 18 rods (convergence) and each rod receives contact from two RB cells (divergence). (B) A representative retinal region with pure photoreceptor degeneration. 'Patchy' areas are characterized by non-functional RB cells (black empty circles) due to degeneration of all rods (black filled circles) within their dendritic field. 'Diffuse' degeneration is characterized by functional RB cells lacking some of their presynaptic rods. Reduction of OS length is schematized in the crosssectional view shown below.

The expected change in the sensitivity of remaining functional RBs due to partial degeneration of rods that were presynaptic to these cells can be formally defined under several simplifying assumptions. First we assume RBs sum their inputs at the rod synapses and thus their sensitivity is proportional to the number of functional dendrites. RB sensitivity would also be proportional to the dark current of each rod, which in turn, would be expected to vary with the outer segment plasma membrane area. We also assume that the signal at each synapse is proportional to the amplification factor achieved in the corresponding ROS. Thus the RB sensitivity, ΔRB_{sens}, as a fraction of control can be defined as:

$$\Delta RB_{sens} = \Delta DEND \cdot \Delta CNG \cdot \Delta ROD_{sens} \quad (6)$$

where $\Delta DEND$ is the fraction of control dendrites still providing input to functional RBs, ΔCNG is the fraction of control CNG channels on rods open in the dark, and ΔROD_{sens} is the fraction of control amplification factor achieved during activation of functional rods. $\Delta DEND$ can be estimated from:

$$\Delta DEND = \frac{\#\,ROD_F \cdot divergence}{\#\,RB_F \cdot convergence} \quad (7)$$

where $\#\,ROD_F$ and $\#\,RB_F$ are the numbers of functional rods and RBs, respectively. The ratio of convergence to divergence is by definition equal to the ratio of the number of rods to RBs in control retinas. Making the appropriate substitutions, we obtain:

$$\Delta RB_{sens} = \frac{\Delta ROD_F \cdot \Delta CNG}{\Delta RB_F} \cdot \Delta ROD_{sens} \quad (8)$$

Assuming use of appropriately saturating light energies and stereotypy of phototransduction activation in all functioning rods, the right-hand side of Eq. (8) can be estimated from experimental parameters as:

$$\Delta RB_{sens} = \frac{\Delta P3_{max}}{\Delta P2_{max}} \cdot \Delta P3_{sens} \quad (9)$$

Note that $\Delta P2_{max}$ must always be equal to or greater than $\Delta P3_{max}$ since we assume pure photoreceptor degeneration (i.e. RB cells do not independently degenerate; they stop functioning only when all of their presynaptic rods degenerate). Furthermore, regional differences in rod OS length is accounted for in the model, as long as $\Delta P3_{max}$ correctly represents total functional CNG channels remaining in any given region.

3.4. Supersensitivity of the P2 component

In normal rats, the observed age-related decline of $P3_{max}$ can be parsimoniously explained by eye growth and loss of rods accompanying senescence (for example, Lai, Jacoby, & Jonas, 1978; Katz & Robison, 1986;

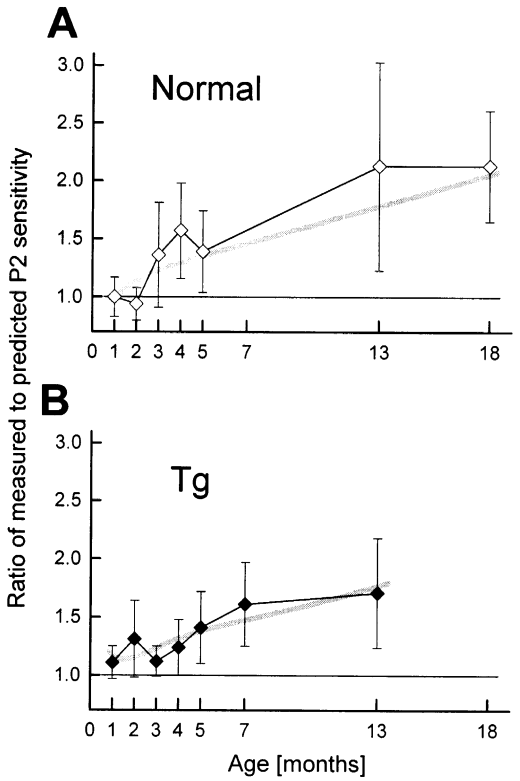

Fig. 5. Ratio of the measured P2 component sensitivity to that predicted by the model of the distal RB pathway in normal (A) and Tg (B) rats as a function of age. Gray lines represent derived values using the double-exponential model of natural history fit to data in Fig. 3. Error bars are 95% confidence intervals.

DiLoreto, Ison, Bowen, Cox, & del Cerro, 1995; Weisse, 1995; Obin et al., 2000); age-related decline of $P2_{max}$ would be consequent to loss of rod input to RB cells. Were the sensitivity parameters of the ERG consistent with this simple hypothesis? We used the mean values of the relevant parameters in 1 month old normal rats as 'control' (in Eq. (9)) to estimate the expected change in RB sensitivity in older normal rats and compared this estimate to the measured $P2_{sens}$ values (Fig. 5A). Measured P2 sensitivities were mostly larger than predicted values; the mean ratio grew from 1.36 (± 0.45) at 3 months to 2.13 (± 0.35) at 18 months. Statistical analysis showed a significant ($P = 0.004$) difference from the theoretical value of 1.

We next determined the ratio of $\Delta P2_{sens}$ to ΔRB_{sens} in Tg rats. For each age, the mean value of ERG parameters in age-matched normal rats was used as 'control' (in Eq. (9)) with one exception; mean values of 5 month-old normal rats were used as control for 7 month-old Tg rat results. On the average, Tg rats had greater $\Delta P2_{sens}$ than that predicted by the model at all ages (Fig. 5B); the mean ratio grew from 1.12 (± 0.13) at 3 months to 1.71 (± 0.47) at 13 months. Statistical analysis showed a significant ($P = 0.0005$) difference from the theoretical value of 1.

4. Discussion

Functional consequences of senescence and degeneration of the rat retina were investigated with ERGs and interpreted with a model of distal RB pathway signaling. Older normal rats showed two-fold greater P2 sensitivity than that predicted by age-related rod loss (Fig. 5A). Tg rats could have an additional 3-fold increase of P2 sensitivity compared to that predicted by progressive rod degeneration; this supersensitivity originated partly at the rod OS (Fig. 3F) and partly at or proximal to the rod-RB synapse (Fig. 5B). Our current understanding of the cellular physiology underlying ERG components combined with previous morphological studies allows the speculation that reactive mechanisms at the rod-RB synapse may be providing augmented RB cell function to compensate for partial loss of photoreceptors in rats.

4.1. Origins of P3 and P2 components of the rat ERG

Two major assumptions are made to interpret the ERG results of the current work. First, we assume that the leading edge of the rat ERG evoked by high-energy stimuli under dark-adapted conditions tracks the suppression of the rod circulating current summed across the retina. Specifically, the saturated P3 amplitude is expected to be proportional to the total number of CNG channels open in the dark and the kinetics of the P3 expected to be defined by amplification achieved by the phototransduction cascade. Theoretical and experimental evidence supports this first major assumption (Penn & Hagins, 1972; Breton et al., 1994; Hood & Birch, 1994; Reiser, Williams, & Pugh, 1996; Pugh et al., 1998; Robson & Frishman, 1999; Machida et al., 2000).

The second major assumption relates the P2 component of the ERG to the activity of RB cells. In the current work, P2 component is defined as the difference between the ERG amplitude and the estimated P3 amplitude at a fixed time of 80 ms following flash stimulus. The saturated P2 amplitude is expected to be proportional to the total number of functional RB cells and the sensitivity of the P2 expected to define the sensitivity of each functional RB cell. The second major assumption is more tenuous than the first assumption but considerable support is provided by recent studies (Gurevich & Slaughter, 1993; Xu & Karwoski, 1994; Robson & Frishman, 1995; Hood & Birch, 1996; Pugh et al., 1998; Lei & Perlman, 1999; Shiells & Falk, 1999; Karwoski & Xu, 1999; Berntson & Taylor, 2000; Euler & Masland, 2000; Kofuji et al., 2000). It may be argued, however, that signaling by more proximal neurons (for example, STR-generators) contaminate the low-intensity region of the P2 component in the rat (Bush et al., 1995; Robson & Frishman, 1995). Tell-tale

signs of STR (negative responses below the b-wave threshold) were not observed in our experiments; this was probably due to protocol difference (Bush et al., 1995; Frishman & Sieving, 1995; Hood & Birch, 1996) and the longer latency of the STR component compared to the 80 ms time chosen for P2 analysis. Furthermore, we did not observe major deviations of P2 amplitude from linearity. Linearity has been taken as evidence of a dominant RB component within the P2 response (Robson & Frishman, 1995; Hood & Birch, 1996) since signals originating at neurons proximal to RB cells have been shown to disturb this linearity (Robson & Frishman, 1995, 1999). Our results showing a high correlation (intercept $= -11.5$ μV, slope $=$ 0.999, $r^2 = 0.89$) between saturated P2 amplitudes estimated at two intensities (-1.2 and $+2.2$ log scot-cd s m^{-2}) would provide further support to our assumption that a single neuronal signal, RB cell activity, was the dominant contributor to the P2 component in the rat. Nevertheless, future studies involving direct measurement of RB activity are of course needed to confirm the indirect ERG findings of the current work.

4.2. Normal aging of the rat retina

Saturated P3 amplitudes of older (18 months) rats were ca. 60% of the value of younger adult (3 months) rats. Age-related loss of rod photoreceptors in the rat retina could be a likely explanation for this reduction (Lai et al., 1978; Katz & Robison, 1986; DiLoreto et al., 1995; Weisse, 1995; Obin et al., 2000). The extent of this loss, especially in albino rats, is strongly related to the light-rearing history of the animals (for example, Lai et al., 1978); the relatively small age-related loss of P3 amplitude observed in the current work is consistent with the relatively dim-light rearing environment used. The sensitivity of the rat P3 component was invariant with age and translated to an amplification factor of ca. 5 s^{-2} similar to that reported in other mammals (Pugh & Lamb, 1993). P2 component function in albino rats did not follow the age-related decline of P3 function and showed a relative retention; P2 saturated amplitude at 18 months was ca. 80% of the value of 3 months and P2 sensitivity increased significantly over this period. We questioned whether a certain spatial distribution of rod loss could account for this combination of physiological results. Our model of distal RB pathway connectivity was not consistent with this hypothesis. An alternative hypothesis involving age-related loss of RB cells (in addition to rods) would also not explain the ERG results since it would predict a further increase in the magnitude of the unaccounted post-receptoral sensitivity. Age-related growth of the globe would be expected to affect P3 and P2 components equally and thus does not explain the relative retention of the P2 function. Differential changes of interstitial conductivity at the photoreceptor versus bipolar layer with age could conceivably account for the apparent retention of P2 function but experimental results supporting such a hypothesis are currently lacking. Another possibility is the existence of an active mechanism that compensates for partial rod loss in aging normal rats by increasing the sensitivity of ERG P2 component. If this hypothesis is valid, it could also apply to degenerative rod loss in the Tg rats.

4.3. Pathophysiology of Tg rats

The most unexpected ERG finding in Tg rats was the supersensitivity of the P3 component. Previously, rod-isolated P3 component sensitivity has been reported to be normal or subnormal in hereditary retinal degenerations of humans (Hood & Birch, 1994; Jacobson et al., 1994; Birch et al., 1995; Jacobson, Cideciyan, Kemp, Sheffield, & Stone, 1996; Cideciyan et al., 1998a; Cideciyan, 2000; Jacobson et al., 2000), mice (Goto et al., 1996; Cheng et al., 1997; Kedzierski, Lloyd, Birch, Bok, & Travis, 1997) and rats (Machida et al., 2000). A normal P3 sensitivity with shortened rod OS length would have been consistent with theoretical considerations that predict an increase in the amplification constant (Pugh & Lamb, 1993) and a decrease in number of photoisomerizations produced for a given level of retinal illuminance (Breton et al., 1994). Experimental results in isolated rat retinas with differing OS lengths have not conflicted with such theoretical considerations (Reiser et al., 1996) although these two factors may not necessarily be balanced. A subnormal P3 sensitivity would have suggested dysfunction of activation mechanisms within rod OS.

Greater than normal P3 sensitivity observed in Tg rats would be consistent with an apparent acceleration of phototransduction activation. This is especially surprising since it is well established that the Tg rat rods have abnormally shortened OS length (Lewin et al., 1998; LaVail et al., 2000; Machida et al., 2000). Several hypotheses can be raised for the apparent acceleration of activation within these short OS. Gradient of light responsiveness has been demonstrated to exist along the length of amphibian OS (for example, Schnapf, 1983; Bandarchi & Leibovic, 1997). If such gradients exist in mammalian rods, shorter rod OS of Tg rats may have biochemical properties more similar to basal end of normal rod OS. The basis of this gradient may involve the age of disks; abnormalities in renewal mechanisms (Liu et al., 1997) could hypothetically change the age gradient of disks along the rod OS of Tg rats. Alternatively, the supersensitivity could involve increased photoisomerizations produced for a given level of illuminance. Overexpression of rhodopsin in these Tg animals could theoretically account for greater photon absorption as long as the mutant rhodopsin is effi-

ciently activated by light; consistent with this hypothesis are transgenic mice that have previously shown a small but significant supersensitivity at the single cell level (Sung, Makino, Bayler, & Nathans, 1994). On the other hand, transgenic VPP mice (carrying a P23H rhodopsin mutation and thus closely approximating the Tg rats in the current study) have shown no evidence of rod photoreceptor supersensitivity (Goto et al., 1996; Wu et al., 1998). Although overexpression of normal bovine opsin has been shown to cause photoreceptor degeneration in transgenic mice, sensitivity measures have not been reported (Tan et al., 2001). Interestingly, a reduction in rhodopsin expression can reduce photoisomerizations but speed up phototransduction activation (Calvert et al., 2001). Effects of self-screening (Baylor & Lamb, 1982; Alpern, Fulton, & Baker, 1987; Makino, Howard, & Williams, 1987) could also conceivably account for the supersensitivity in shortened rod OS. Our preliminary results set the stage for further experiments that can eliminate some of these many alternatives.

The most immediately recognizable feature (that did not require special analyses) of a typical Tg rat ERG was a small a-wave and a large b-wave (Fig. 2). Quantitative analyses showed normal or near-normal P2 amplitude and sensitivity associated with large reductions with P3 amplitudes. The ratio of P2 to P3 amplitude was ca. three times greater than normal. Application of a model of distal RB pathway signaling showed that the supersensitivity of the P3 component only partially accounted for the observed P2 results and suggested the existence of an additional compensatory mechanism acting to augment post-receptoral function in Tg rats; parsimony would dictate this mechanism to be similar to that seen in aging normal rats.

4.4. Interpretation of ERG results with models of retinal connectivity and signaling

To our knowledge, three models have been previously used to interpret experimentally measured changes in P3 and P2 components of the rod-isolated ERG in terms of the underlying pathophysiology (Hood & Birch, 1992; Hood et al., 1994; Cideciyan et al., 1998a); all three models have been applied only to human ERG data from normal subjects and patients with hereditary retinal degenerations. The model developed in the current work follows the theoretical framework provided by Hood and Birch, i.e. rod-isolated ERG consists of the linear summation of P3 and P2 components. A significant difference between the current model and that of Hood and Birch is the range of temporal validity. Hood and Birch use a dynamic model of the P2 component that attempts to describe the full ERG waveform and is specifically optimized to describe trough-to-peak (time-variant) P2 component amplitude and timing data from human ERGs. The correspondence between the model and measured data may not be close at any given fixed time. Current model uses a simpler static model of the P2 component that describes the measured amplitude data very well at the fixed time chosen. Our choice of the static model was based on recent results suggesting easier interpretation of amplitudes measured at a fixed time on the leading edge of the ERG b-wave (Robson & Frishman, 1995, 1999).

It has been previously shown that when there are large regional variations of photoreceptor sensitivity and appropriately saturating stimulus intensities cannot be used due to technical limitations, assumption of a homogeneous degenerative process across the retina can lead to wrong inferences about the underlying pathophysiology (Hood et al., 1993, 1994). In the current work, both P3 and P2 components did not show evidence of lack of saturation. Specifically for example, the implicit time of the maximal a-wave in Tg rats was equal or shorter than that in normal rats. If we can assume that P3 component of normal rats was saturated, then we have to assume that Tg rat results were also saturated. The close correspondence of saturated P2 amplitudes across a 3 log unit stimulus range allows a similar argument for the P2 component.

The model of distal RB pathway connectivity and signaling developed in the current work provides a simple analytical expression (Eq. (9)) for the expected change of RB cell sensitivity as a function of changes in receptor sensitivity, receptor CNG channels and RB number estimated from appropriately recorded ERG parameters. The model is independent from the specific spatial pattern of photoreceptor degeneration based on recent work suggesting the existence of both 'patchy' and 'diffuse' components to some rhodopsin-associated human retinal degenerations (Cideciyan et al., 1998a). Previous simulations have considered the relationship between P2 and P3 amplitudes in humans but the effect of P2 and P3 sensitivities have not been evaluated (Cideciyan et al., 1998a).

4.5. The basis of the post-receptoral compensatory mechanism

Augmented post-receptoral function may not be specific to the aging normal and Tg rats considered in the current study. ERG analyses of mice with slow retinal degeneration caused by *rds* mutations (Kedzierski et al., 1997), rats with mild and moderate light damage (Noell, 1980; Sugawara et al., 2000) and two lines of transgenic rats (Machida et al., 2000) have also shown relative preservation of post-receptoral function. Anatomical studies (performed independently) in some of these animal models of partial photoreceptor loss have provided clues to the basis of this presumably

common compensatory mechanism. Specifically, dramatic increases have been observed in the number of rod terminals showing multiple synaptic ribbons in normal aging of mice, *rds* homozygous and heterozygous mutant mice, chimaeric mice of *rd* and wild-type combination and albino mice exposed to constant light (Jansen & Sanyal, 1987, 1992; Sanyal, Hawkins, Jansen, & Zeilmaker, 1992; Jansen et al., 1997). Three-dimensional reconstruction has shown that this proliferation of synaptic sites occurs through sprouting from the processes already present within the terminals (Jansen et al., 1997). The existence of similar synaptic changes in Tg rats remains to be proven in future studies.

What would be the physiological consequences of reactive changes occurring at the rod synapses? It is well established that a tonically active inward current is shut off by light and glutamate, in rods and RB cells, respectively (Nawy & Jahr, 1990; Robson & Frishman, 1995). In darkness, glutamate levels in the rod-RB synapse are high and cation channels of RB cells are closed. Light-induced shut-off of rod photoreceptor cation channels decreases glutamate release at the synapse and opens the cation channels of RB cells. A simple analysis would argue that two synaptic ribbons at each dendrite would effectively double the synaptic gain within the linear range. More elaborate analyses (see for example, van Rossum & Smith, 1998) are beyond the scope of the current work.

If one accepts the view that mammalian retina does possess structural plasticity at the first synapse of the visual system, it is not unreasonable to hypothesize that similar changes may also occur at more proximal synapses. It has been reported, for example, that elevation of b-wave thresholds can be significantly greater than the elevations in STR threshold in RCS (Bush et al., 1995) and light damaged rats (Sugawara et al., 2000). Similarly, young Labrador retriever dogs homozygous and heterozygous for late onset rod-cone degeneration can show normal STR signals at a time when they have dramatically abnormal ERG b-waves (Kommonen, Kylma, Karhunen, Dawson, & Penn, 1997). These results could represent functional correlates of reactive changes occurring at the inner plexiform layer under the assumption that STR generators are more proximal to the P2 generators.

It is well accepted that cell-cell interactions are required for the viability of neurons in the retina, and as a consequence, a primary insult to a specific photoreceptor population can induce secondary changes in neighboring or connected neurons. There have been several examples where degeneration of rods causes synaptic abnormalities (for example, Blanks, Adinolfi, & Lolley, 1974; Nomura et al., 1994; Li et al., 1998b; Strettoi & Pignatelli, 2000) and exaggerates the visual deficit from the primary pathology. The current study focused on the opposite effect: compensatory synaptogenesis in reaction to partial loss of rods. The degree of visual benefit resulting from this presumably self-protective mechanism may be expected to depend on the species, the synapse, the trophic interactions of the cells involved, as well as the type, extent and natural history of the primary insult. If reactive synaptogenesis is also occurring in human retinal degenerations, current methods of monitoring natural history of disease and planned therapies may require careful reconsideration.

Acknowledgements

We thank Robert G. Smith for helpful comments and discussions. Mequi Jiang, Jiancheng Huang and Erica Dale provided valuable help with the studies. Supported by the Foundation Fighting Blindness, Incorporated, National Institutes of Health (EY-05627, -13203, -01919, -06842, -01583), The F.M. Kirby Foundation and the Mackall Trust. MML and SGJ are Research to Prevent Blindness Senior Scientific Investigators. AVC is a Research to Prevent Blindness William and Mary Greve Scholar.

References

Alpern, M., Fulton, A. B., & Baker, B. N. (1987). 'Self-screening' of rhodopsin in rod outer segments. *Vision Research*, *27*, 1459–1470.

Ashmore, J. F., & Falk, G. (1980). Responses of rod bipolar cells in the dark-adapted retina of the dogfish, *Scyliorhinus canicula*. *Journal of Physiology*, *300*, 115–150.

Bandarchi, J., & Leibovic, K. N. (1997). Effects of animal age on the responses along the outer segment of retinal rod photoreceptors. *Neuroreport*, *8*, 581–585.

Banin, E., Cideciyan, A. V., Aleman, T. S., Petters, R. M., Wong, F., Milam, A. H., & Jacobson, S. G. (1999). Retinal rod photoreceptor-specific gene mutation perturbs cone pathway development. *Neuron*, *23*, 549–557.

Baylor, D. A., & Lamb, T. D. (1982). Local effects of bleaching in retinal rods of the toad. *Journal of Physiology*, *328*, 49–71.

Berntson, A., & Taylor, W. R. (2000). Response characteristics and receptive field widths of on-bipolar cells in the mouse retina. *Journal of Physiology*, *524*, 879–889.

Berson, E. L., Sandberg, M. A., Rosner, B., Birch, D. G., & Hanson, A. H. (1985). Natural course of retinitis pigmentosa over a three-year interval. *American Journal of Ophthalmology*, *99*, 240–251.

Birch, D. G., Hood, D. C., Nusinowitz, S., & Pepperberg, D. R. (1995). Abnormal activation and inactivation mechanisms of rod transduction in patients with autosomal dominant retinitis pigmentosa and the pro-23-his mutation. *Investigative Ophthalmology and Visual Science*, *36*, 1603–1614.

Birch, D. G., Anderson, J. L., & Fish, G. E. (1999). Yearly rates of rod and cone functional loss in retinitis pigmentosa and cone-rod dystrophy. *Ophthalmology*, *106*, 258–268.

Blanks, J. C., Adinolfi, A. M., & Lolley, R. N. (1974). Photoreceptor degeneration and synaptogenesis in retinal-degenerative (rd) mice. *Journal of Comparative Neurology*, *156*, 95–106.

Blackmon, S. M., Peng, Y.-W., Hao, Y., Moon, S. J., Oliveira, L. B., Tatebayashi, M., Petters, R. M., & Wong, F. (2000). Early loss of synaptic protein PSD-95 from rod terminals of rhodopsin P347L transgenic porcine retina. *Brain Research*, *885*, 53–61.

Boycott, B. B., & Dowling, J. E. (1969). Organization of the primate retina: light microscopy. *Philosophical Transactions of the Royal Society London B*, *799*, 109–194.

Breton, M. E., Schueller, A. W., Lamb, T. D., & Pugh, E. N. Jr (1994). Analysis of ERG a-wave amplification and kinetics in terms of the G-protein cascade of phototransduction. *Investigative Ophthalmology and Visual Science*, *35*, 295–309.

Bush, R. A., Hawks, K. W., & Sieving, P. A. (1995). Preservation of inner retinal responses in the aged Royal College of Surgeons rat. Evidence against glutamate excitotoxicity in photoreceptor degeneration. *Investigative Ophthalmology and Visual Science*, *36*, 2054–2062.

Calderone, L., Grimes, P., & Shalev, M. (1986). Acute reversible cataract induced by xylazine and by ketamine–xylazine anesthesia in rats and mice. *Experimental Eye Research*, *42*, 331–337.

Calvert, P. D., Govardovskii, V. I., Krasnoperova, N., Anderson, R. E., Lem, J., & Makino, C. L. (2001). Membrane protein diffusion sets the speed of rod phototransduction. *Nature*, *411*, 90–94.

Chang, G. Q., Hao, Y., & Wong, F. (1993). Apoptosis: final common pathway of photoreceptor death in rd, rds, and rhodopsin mutant mice. *Neuron*, *11*, 595–605.

Chen, C. K., Burns, M. E., Spencer, M., Niemi, G. A., Chen, J., Hurley, J. B., Baylor, D. A., & Simon, M. I. (1999). Abnormal photoresponses and light-induced apoptosis in rods lacking rhodopsin kinase. *Proceedings of the National Academy of Sciences USA*, *96*, 3718–3722.

Chen, J., Makino, C. L., Peachey, N. S., Baylor, D. A., & Simon, M. I. (1995). Mechanisms of rhodopsin inactivation in vivo as revealed by a COOH-terminal truncation mutant. *Science*, *267*, 374–377.

Cheng, T., Peachey, N. S., Li, S., Goto, Y., Cao, Y., & Naash, M. I. (1997). The effect of peripherin/rds haploinsufficiency on rod and cone photoreceptors. *Journal of Neuroscience*, *17*, 8118–8128.

Cideciyan, A. V. (2000). In vivo assessment of photoreceptor function in human diseases caused by photoreceptor-specific gene mutations. *Methods in Enzymology*, *316*, 611–626.

Cideciyan, A. V., & Jacobson, S. G. (1993). Negative electroretinograms in retinitis pigmentosa. *Investigative Ophthalmology and Visual Science*, *34*, 3253–3263.

Cideciyan, A. V., & Jacobson, S. G. (1996). An alternative phototransduction model for human rod and cone ERG a-waves: normal parameters and variation with age. *Vision Research*, *36*, 2609–2621.

Cideciyan, A. V., Hood, D. C., Huang, Y., Banin, E., Li, Z. Y., Stone, E. M., Milam, A. H., & Jacobson, S. G. (1998a). Disease sequence from mutant rhodopsin allele to rod and cone photoreceptor degeneration in man. *Proceedings of the National Academy of Sciences USA*, *95*, 7103–7108.

Cideciyan, A. V., Zhao, X., Nielsen, L., Khani, S. C., Jacobson, S. G., & Palczewski, K. (1998b). Null mutation in the rhodopsin kinase gene slows recovery kinetics of rod and cone phototransduction in man. *Proceedings of the National Academy of Sciences USA*, *95*, 328–333.

Cideciyan, A. V., Aleman, T. S., Jiang, M., Montemayor, R., Wen, R., Laties, A. M., LaVail, M. M., & Jacobson, S. G. (1999a). Early mechanism of rod dysfunction in the rhodopsin P23H transgenic rat model of retinitis pigmentosa. *Investigative Ophthalmology and Visual Science (Supplement)*, *40*, S24 (Abstract).

Cideciyan, A. V., Aleman, T. S., Bennett, J., & Banin, E. (1999b). Comparative study of mammalian phototransduction in vivo: a prelude to preclinical treatment trials in retinal degenerations. In *Vision science and its applications* (pp. 60–63). Washington, DC: OSA Technical Digest, Optical Society of America.

Clarke, G., Heon, E., & McInnes, R. R. (2000a). Recent advances in the molecular basis of inherited photoreceptor degeneration. *Clinical Genetics*, *57*, 313–329.

Clarke, G., Collins, R. A., Leavitt, B. R., Andrews, D. F., Hayden, M. R., Lumsden, C. J., & McInnes, R. R. (2000b). A one-hit model of cell death in inherited neuronal degenerations. *Nature*, *406*, 195–199.

Cone, R. A. (1963). Quantum relations of the rat electroretinogram. *Journal of General Physiology*, *46*, 1267–1286.

Cotman, C. W., & Nieto-Sampedro, M. (1984). Cell biology of synaptic plasticity. *Science*, *225*, 1287–1294.

Cowan, W. M. (1970). Anterograde and retrograde transneuronal degeneration in the central and peripheral nervous system. In W. J. Nauta, & S. O. E. Ebbesson, *Contemporary research methods in neuroanatomy* (pp. 217–251). New York: Springer.

Deegan, J. F. II, & Jacobs, G. H. (1993). On the identity of the cone types of the rat retina. *Experimental Eye Research*, *56*, 375–377.

DiLoreto, D. Jr, Ison, J. R., Bowen, G. P., Cox, C., & del Cerro, M. (1995). A functional analysis of the age-related degeneration in the Fischer 344 rat. *Current Eye Research*, *14*, 303–310.

Dryja, T. P., McGee, T. L., Reichel, E., Hahn, L. B., Cowley, G. S., Yandell, D. W., Sandberg, M. A., & Berson, E. L. (1990). A point mutation of the rhodopsin gene in one form of retinitis pigmentosa. *Nature*, *343*, 364–366.

Euler, T., & Masland, R. H. (2000). Light-evoked responses of bipolar cells in a mammalian retina. *Journal of Neurophysiology*, *83*, 1817–1829.

Euler, T., & Wassle, H. (1995). Immunocytochemical identification of cone bipolar cells in the rat retina. *Journal of Comparative Neurology*, *361*, 461–478.

Fariss, R. N., Li, Z. Y., & Milam, A. H. (2000). Abnormalities in rod photoreceptors, amacrine cells, and horizontal cells in human retinas with retinitis pigmentosa. *American Journal of Ophthalmology*, *129*, 215–223.

Frishman, L. J., & Sieving, P. A. (1995). Evidence for two sites of adaptation affecting the dark-adapted ERG of cats and primates. *Vision Research*, *35*, 435–442.

Fulton, A. B., Hansen, R. M., & Findl, O. (1995). The development of the rod photoresponse from dark-adapted rats. *Investigative Ophthalmology and Visual Science*, *36*, 1038–1045.

Gal, A., Apfelstedt-Sylla, E., Janecke, A. R., & Zrenner, E. (1997). Rhodopsin mutations in inherited retinal dystrophies and dysfunctions. *Progress in Retinal and Eye Research*, *16*, 51–79.

Goto, Y., Peachey, N. S., Ziroli, N. E., Seiple, W. H., Gryczan, C., Pepperberg, D. R., & Naash, M. I. (1996). Rod phototransduction in transgenic mice expressing a mutant opsin gene. *Journal of the Optical Society of America A*, *13*, 577–585.

Granit, R. (1933). The components of the retinal action potential in mammals and their relation to the discharge in the optic nerve. *Journal of Physiology*, *77*, 207–239.

Green, D. G., Herreros de Tejada, P., & Glover, M. J. (1991). Are albino rats night blind? *Investigative Ophthalmology and Visual Science*, *32*, 2366–2371.

Grunert, U., & Martin, P. R. (1991). Rod bipolar cells in the macaque monkey retina: immunoreactivity and connectivity. *Journal of Neuroscience*, *11*, 2742–2758.

Gurevich, L., & Slaughter, M. M. (1993). Comparison of the waveforms of the ON bipolar neuron and the b-wave of the electroretinogram. *Vision Research*, *33*, 2431–2435.

Hetling, J. R., & Pepperberg, D. R. (1999). Sensitivity and kinetics of mouse rod flash responses determined in vivo from paired-flash electroretinograms. *Journal of Physiology*, *516*, 593–609.

Hood, D. C., & Birch, D. G. (1992). A computational model of the amplitude and implicit time of the b-wave of the human ERG. *Visual Neuroscience*, *8*, 107–126.

Hood, D. C., & Birch, D. G. (1994). Rod phototransduction in retinitis pigmentosa: estimation and interpretation of parameters

derived from the rod a-wave. *Investigative Ophthalmology and Visual Science*, *35*, 2948–2961.

Hood, D. C., & Birch, D. G. (1996). B-wave of the scotopic (rod) electroretinogram as a measure of the activity of human on-bipolar cells. *Journal of the Optical Society of America A*, *13*, 623–633.

Hood, D. C., & Greenstein, V. (1990). Models of the normal and abnormal rod system. *Vision Research*, *30*, 51–68.

Hood, D. C., Shady, S., & Birch, D. G. (1993). Heterogeneity in retinal disease and the computational model of the human-rod response. *Journal of the Optical Society of America A*, *10*, 1624–1630.

Hood, D. C., Shady, S., & Birch, D. G. (1994). Understanding changes in the b-wave of the ERG caused by heterogeneous receptor damage. *Investigative Ophthalmology and Visual Science*, *35*, 2477–2488.

Humphries, M. M., Rancourt, D., Farrar, G. J., Kenna, P., Hazel, M., Bush, R. A., Sieving, P. A., Sheils, D. M., McNally, N., Creighton, P., Erven, A., Boros, A., Gulya, K., Capecchi, M. R., & Humphries, P. (1997). Retinopathy induced in mice by targeted disruption of the rhodopsin gene. *Nature Genetics*, *15*, 216–219.

Jacobson, S. G., Kemp, C. M., Sung, C. H., & Nathans, J. (1991). Retinal function and rhodopsin levels in autosomal dominant retinitis pigmentosa with rhodopsin mutations. *American Journal of Ophthalmology*, *112*, 256–271.

Jacobson, S. G., Kemp, C. M., Cideciyan, A. V., Macke, J. P., Sung, C. H., & Nathans, J. (1994). Phenotypes of stop codon and splice site rhodopsin mutations causing retinitis pigmentosa. *Investigative Ophthalmology and Visual Science*, *35*, 2521–2534.

Jacobson, S. G., Cideciyan, A. V., Kemp, C. M., Sheffield, V. C., & Stone, E. M. (1996). Photoreceptor function in heterozygotes with insertion or deletion mutations in the RDS gene. *Investigative Ophthalmology and Visual Science*, *37*, 1662–1674.

Jacobson, S. G., Cideciyan, A. V., Iannaccone, A., Weleber, R. G., Fishman, G. A., Maguire, A. M., Affatigato, L. M., Bennett, J., Pierce, E. A., Danciger, M., Farber, D. B., & Stone, E. M. (2000). Disease expression of RP1 mutations causing autosomal dominant retinitis pigmentosa. *Investigative Ophthalmology and Visual Science*, *41*, 1898–1908.

Jansen, H. G., & Sanyal, S. (1987). Synaptic changes in the terminals of rod photoreceptors of albino mice after partial visual cell loss induced by brief exposure to constant light. *Cell and Tissue Research*, *250*, 43–52.

Jansen, H. G., & Sanyal, S. (1992). Synaptic plasticity in the rod terminals after partial photoreceptor cell loss in the heterozygous rds mutant mouse. *Journal of Comparative Neurology*, *316*, 117–125.

Jansen, H. G., Hawkins, R. K., & Sanyal, S. (1997). Synaptic growth in the rod terminals of mice after partial photoreceptor cell loss: a three-dimensional ultrastructural study. *Microscopy Research and Technique*, *36*, 96–105.

Jeon, C. J., Strettoi, E., & Masland, R. H. (1998). The major cell populations of the mouse retina. *Journal of Neuroscience*, *18*, 8936–8946.

Karwoski, C. J., & Xu, X. (1999). Current source-density analysis of light-evoked field potentials in rabbit retina. *Visual Neuroscience*, *16*, 369–377.

Katz, M. L., & Robison, W. G. Jr (1986). Evidence of cell loss from the rat retina during senescence. *Experimental Eye Research*, *42*, 293–304.

Kedzierski, W., Lloyd, M., Birch, D. G., Bok, D., & Travis, G. H. (1997). Generation and analysis of transgenic mice expressing P216L-substituted rds/peripherin in rod photoreceptors. *Investigative Ophthalmology and Visual Science*, *38*, 498–509.

Kemp, C. M., Jacobson, S. G., Roman, A. J., Sung, C. H., & Nathans, J. (1992). Abnormal rod dark adaptation in autosomal dominant retinitis pigmentosa with proline-23-histidine rhodopsin mutation. *American Journal of Ophthalmology*, *113*, 165–174.

Kofuji, P., Ceelen, P., Zahs, K. R., Surbeck, L. W., Lester, H. A., & Newman, E. A. (2000). Genetic inactivation of an inwardly rectifying potassium channel (Kir4.1 subunit) in mice: phenotypic impact in retina. *Journal of Neuroscience*, *20*, 5733–5740.

Kolb, H., & Gouras, P. (1974). Electron microscopic observations of human retinitis pigmentosa, dominantly inherited. *Investigative Ophthalmology*, *13*, 487–498.

Kommonen, B., Kylma, T., Karhunen, U., Dawson, W. W., & Penn, J. S. (1997). Impaired retinal function in young labrador retriever dogs heterozygous for late onset rod–cone degeneration. *Vision Research*, *37*, 365–370.

Lai, Y. L., Jacoby, R. O., & Jonas, A. M. (1978). Age-related and light-associated retinal changes in Fischer rats. *Investigative Ophthalmology and Visual Science*, *17*, 634–638.

Lamb, T. D., & Pugh, E. N. Jr (1992). A quantitative account of the activation steps involved in phototransduction in amphibian photoreceptors. *Journal of Physiology*, *449*, 719–758.

Lei, B., & Perlman, I. (1999). The contributions of voltage- and time-dependent potassium conductances to the electroretinogram in rabbits. *Visual Neuroscience*, *16*, 743–754.

LaVail, M. M., Yasumura, D., Matthes, M. T., Drenser, K. A., Flannery, J. G., Lewin, A. S., & Hauswirth, W. W. (2000). Ribozyme rescue of photoreceptor cells in P23H transgenic rats: long-term survival and late-stage therapy. *Proceedings of the National Academy of Sciences USA*, *97*, 11488–11493.

Lewin, A. S., Drenser, K. A., Hauswirth, W. W., Nishikawa, S., Yasumura, D., Flannery, J. G., & LaVail, M. M. (1998). Ribozyme rescue of photoreceptor cells in a transgenic rat model of autosomal dominant retinitis pigmentosa. *Nature Medicine*, *4*, 967–971.

Li, T., Snyder, W. K., Olsson, J. E., & Dryja, T. P. (1996). Transgenic mice carrying the dominant rhodopsin mutation P347S: evidence for defective vectorial transport of rhodopsin to the outer segments. *Proceedings of the National Academy of Sciences USA*, *93*, 14176–14181.

Li, T., Sandberg, M. A., Pawlyk, B. S., Rosner, B., Hayes, K. C., Dryja, T. P., & Berson, E. L. (1998a). Effect of vitamin A supplementation on rhodopsin mutants threonine-17 → methionine and proline-347 → serine in transgenic mice and in cell cultures. *Proceedings of the National Academy of Sciences USA*, *95*, 11933–11938.

Li, Z. Y., Jacobson, S. G., & Milam, A. H. (1994). Autosomal dominant retinitis pigmentosa caused by the threonine-17-methionine rhodopsin mutation: retinal histopathology and immunocytochemistry. *Experimental Eye Research*, *58*, 397–408.

Li, Z. Y., Kljavin, I. J., & Milam, A. H. (1995). Rod photoreceptor neurite sprouting in retinitis pigmentosa. *Journal of Neuroscience*, *15*, 5429–5438.

Li, Z. Y., Wong, F., Chang, J. H., Possin, D. E., Hao, Y., Petters, R. M., & Milam, A. H. (1998b). Rhodopsin transgenic pigs as a model for human retinitis pigmentosa. *Investigative Ophthalmology and Visual Science*, *39*, 808–819.

Littell, R. C., Milliken, G. A., Stroup, W. W., & Wolfinger, R. D. (1996). *SAS system for mixed models*. Cary, NC: SAS Institute Incorporated.

Liu, X., Wu, T. H., Stowe, S., Matsushita, A., Arikawa, K., Naash, M. I., & Williams, D. S. (1997). Defective phototransductive disk membrane morphogenesis in transgenic mice expressing opsin with a mutated N-terminal domain. *Journal of Cell Science*, *110*, 2589–2597.

Lyubarsky, A. L., Falsini, B., Pennesi, M. E., Valentini, P., & Pugh, E. N. Jr (1999). UV- and midwave-sensitive cone-driven retinal responses of the mouse: a possible phenotype for coexpression of cone photopigments. *Journal of Neuroscience*, *19*, 442–455.

Lyubarsky, A. L., Chen, C., Simon, M. I., & Pugh, E. N. (2000). Mice lacking G-protein receptor kinase 1 have profoundly slowed recovery of cone-driven retinal responses. *Journal of Neuroscience*, *20*, 2209–2217.

Machida, S., Kondo, M., Jamison, J. A., Khan, N. W., Kononen, L. T., Sugawara, T., Bush, R. A., & Sieving, P. A. (2000). P23H Rhodopsin transgenic rat: correlation of retinal function with histopathology. *Investigative Ophthalmology and Visual Science*, *41*, 3200–3209.

Makino, C. L., Howard, L. N., & Williams, T. P. (1987). Intracellular topography of rhodopsin bleaching. *Science*, *238*, 1716–1717.

Massof, R. W., & Finkelstein, D. (1987). A two-stage hypothesis for the natural course of retinitis pigmentosa. In E. Zrenner, H. Krastel, & H.-H. Goebel, *Research in retinitis pigmentosa* (pp. 29–58). Oxford: Pergamon Press.

Milam, A. H., Li, Z. Y., Cideciyan, A. V., & Jacobson, S. G. (1996). Clinicopathologic effects of the Q64ter rhodopsin mutation in retinitis pigmentosa. *Investigative Ophthalmology and Visual Science*, *37*, 753–765.

Naarendorp, F., & Williams, G. E. (1999). The d-wave of the rod electroretinogram of rat originates in the cone pathway. *Visual Neuroscience*, *16*, 91–105.

Naash, M. I., Hollyfield, J. G., al-Ubaidi, M. R., & Baehr, W. (1993). Simulation of human autosomal dominant retinitis pigmentosa in transgenic mice expressing a mutated murine opsin gene. *Proceedings of the National Academy of Sciences USA*, *90*, 5499–5503.

Nawy, S., & Jahr, C. E. (1990). Suppression by glutamate of cGMP-activated conductance in retinal bipolar cells. *Nature*, *346*, 269–271.

Noell, W. K. (1980). There are different kinds of retinal light damage in the rat. In T. P. Williams, & B. N. Baker, *The effect of constant light on visual processes* (pp. 3–28). New York: Plenum.

Nomura, A., Shigemoto, R., Nakamura, Y., Okamoto, N., Mizuno, N., & Nakanishi, S. (1994). Developmentally regulated postsynaptic localization of a metabotropic glutamate receptor in rat rod bipolar cells. *Cell*, *77*, 361–369.

Nusinowitz, S., Azimi, A., & Heckenlively, J. R. (2000). Adaptation, body temperature, pupil size, and anesthetic effects on the electroretinogram (ERG) in mice. *Investigative Ophthalmology and Visual Science (Supplement)*, *41*, S495 (Abstract).

Obin, M., Pike, A., Halbleib, M., Lipman, R., Taylor, A., & Bronson, R. (2000). Calorie restriction modulates age-dependent changes in the retinas of Brown Norway rats. *Mechamisms of Ageing and Development*, *114*, 133–147.

Olsson, J. E., Gordon, J. W., Pawlyk, B. S., Roof, D., Hayes, A., Molday, R. S., Mukai, S., Cowley, G. S., Berson, E. L., & Dryja, T. P. (1992). Transgenic mice with a rhodopsin mutation (Pro23His): a mouse model of autosomal dominant retinitis pigmentosa. *Neuron*, *9*, 815–830.

Organisciak, D. T., Darrow, R. M., Barsalou, L., Darrow, R. A., Kutty, R. K., Kutty, G., & Wiggert, B. (1998). Light history and age-related changes in retinal light damage. *Investigative Ophthalmology and Visual Science*, *39*, 1107–1116.

Peng, Y. W., Hao, Y., Petters, R. M., & Wong, F. (2000). Ectopic synaptogenesis in the mammalian retina caused by rod photoreceptor-specific mutations. *Nature Neuroscience*, *3*, 1121–1127.

Penn, R. D., & Hagins, W. A. (1972). Kinetics of the photocurrent of retinal rods. *Biophysical Journal*, *12*, 1073–1094.

Pennesi, M. E., Lyubarsky, A. L., & Pugh, E. N. Jr (1998). Extreme responsiveness of the pupil of the dark-adapted mouse to steady retinal illumination. *Investigative Ophthalmology and Visual Science*, *39*, 2148–2156.

Pepperberg, D. R. (1998). Does rod phototransduction involve the delayed transition of activated rhodopsin to a second, more active catalytic state? *Visual Neuroscience*, *15*, 1067–1078.

Pepperberg, D. R., Birch, D. G., Hofmann, K. P., & Hood, D. C. (1996). Recovery kinetics of human rod phototransduction inferred from the two-branched α-wave saturation function. *Journal of the Optical Society of America A*, *13*, 586–600.

Pepperberg, D. R., Birch, D. G., & Hood, D. C. (2000). Electroretinographic determination of human rod flash response in vivo. *Methods in Enzymology*, *316*, 202–223.

Petters, R. M., Alexander, C. A., Wells, K. D., Collins, E. B., Sommer, J. R., Blanton, M. R., Rojas, G., Hao, Y., Flowers, W. L., Banin, E., Cideciyan, A. V., Jacobson, S. G., & Wong, F. (1997). Genetically engineered large animal model for studying cone photoreceptor survival and degeneration in retinitis pigmentosa. *Natural Biotechnology*, *15*, 965–970.

Phelan, J. K., & Bok, D. (2000). A brief review of retinitis pigmentosa and the identified retinitis pigmentosa genes. *Molecular Vision*, *6*, 116–124.

Portera-Cailliau, C., Sung, C. H., Nathans, J., & Adler, R. (1994). Apoptotic photoreceptor cell death in mouse models of retinitis pigmentosa. *Proceedings of the National Academy of Sciences USA*, *91*, 974–978.

Pugh, E. N. Jr, & Lamb, T. D. (1993). Amplification and kinetics of the activation steps in phototransduction. *Biochimica et Biophysica Acta*, *1141*, 111–149.

Pugh, E. N. Jr, Falsini, B., & Lyubarsky, A. L. (1998). The origin of the major rod- and cone-driven components of the rodent electroretinogram and the effect of age and light-rearing history on the magnitude of these components. In T. P. Williams, & A. B. Thistle, *Photostasis and related phenomena* (pp. 93–128). New York: Plenum.

Rattner, A., Sun, H., & Nathans, J. (1999). Molecular genetics of human retinal disease. *Annual Review of Genetics*, *33*, 89–131.

Reiser, M. A., Williams, T. P., & Pugh, E. N. Jr (1996). The effect of light history on the aspartate-isolated fast-PIII responses of the albino rat retina. *Investigative Ophthalmology and Visual Science*, *37*, 221–229.

Robson, J. G., & Frishman, L. J. (1995). Response linearity and kinetics of the cat retina: the bipolar cell component of the dark-adapted electroretinogram. *Visual Neuroscience*, *12*, 837–850.

Robson, J. G., & Frishman, L. J. (1999). Dissecting the dark-adapted electroretinogram. *Documenta Ophthalmologica*, *95*, 187–215.

van Rossum, M. C., & Smith, R. G. (1998). Noise removal at the rod synapse of mammalian retina. *Visual Neuroscience*, *15*, 809–821.

Sanyal, S., Hawkins, R. K., Jansen, H. G., & Zeilmaker, G. H. (1992). Compensatory synaptic growth in the rod terminals as a sequel to partial photoreceptor cell loss in the retina of chimaeric mice. *Development*, *114*, 797–803.

Schnapf, J. L. (1983). Dependence of the single photon response on longitudinal position of absorption in toad rod outer segments. *Journal of Physiology*, *343*, 147–159.

Sherrard, R. M., & Bower, A. J. (1998). Role of afferents in the development and cell survival of the vertebrate nervous system. *Clinical and Experimental Pharmacology and Physiology*, *25*, 487–495.

Shiells, R. A., & Falk, G. (1999). Contribution of rod, on-bipolar, and horizontal cell light responses to the ERG of dogfish retina. *Visual Neuroscience*, *16*, 503–511.

Shinowara, N. L., London, E. D., & Rapoport, S. I. (1982). Changes in retinal morphology and glucose utilization in aging albino rats. *Experimental Eye Research*, *34*, 517–530.

Smith, R. G., Freed, M. A., & Sterling, P. (1986). Microcircuitry of the dark-adapted cat retina: functional architecture of the rod–cone network. *Journal of Neuroscience*, *6*, 3505–3517.

Steinberg, R. H., Flannery, J. G., Naash, M., Oh, P., Matthes, M. T., Yasumura, D., Lau-Villacorta, C., Chen, J., & LaVail, M. M. (1996). Transgenic rat models of inherited retinal degeneration caused by mutant opsin genes. *Investigative Ophthalmology and Visual Science (Supplment)*, *37*, S698 (Abstract).

Strettoi, E., & Pignatelli, V. (2000). Modifications of retinal neurons in a mouse model of retinitis pigmentosa. *Proceedings of the National Academy of Sciences USA*, *97*, 11020–11025.

Sugawara, T., Sieving, P. A., & Bush, R. A. (2000). Quantitative relationship of the scotopic and photopic ERG to photoreceptor cell loss in light damaged rats. *Experimental Eye Research*, *70*, 693–705.

Sung, C. H., Makino, C., Baylor, D., & Nathans, J. (1994). A rhodopsin gene mutation responsible for autosomal dominant retinitis pigmentosa results in a protein that is defective in localization to the photoreceptor outer segment. *Journal of Neuroscience*, *14*, 5818–5833.

Tan, E., Wang, Q., Quiamboa, A. B., Xu, X., Qtaishat, N. M., Peachey, N. S., Lem, J., Fliesler, S. J., Pepperberg, D. R., Naash, M. I., & Al-Ubaidi, M. R. (2001). The relationship between opsin overexpression and photoreceptor degeneration. *Investigative Ophthalmology and Visual Science*, *42*, 589–600.

Toda, K., Bush, R. A., Humphries, P., & Sieving, P. A. (1999). The electroretinogram of the rhodopsin knockout mouse. *Visual Neuroscience*, *16*, 391–398.

Tucker, G. S., & Jacobson, S. G. (1988). Morphological findings in retinitis pigmentosa with early diffuse rod dysfunction. *Retina*, *8*, 30–41.

Van Hooser, J. P., Aleman, T. S., He, Y. G., Cideciyan, A. V., Kuksa, V., Pittler, S. J., Stone, E. M., Jacobson, S. G., & Palczewski, K. (2000). Rapid restoration of visual pigment and function with oral retinoid in a mouse model of childhood blindness. *Proceedings of the National Academy of Sciences USA*, *97*, 8623–8628.

Weisse, I. (1995). Changes in the aging rat retina. *Ophthalmic Research*, *27*, 154–163.

Weller, R. E., & Kaas, J. H. (1989). Parameters affecting the loss of ganglion cells of the retina following ablations of striate cortex in primates. *Visual Neuroscience*, *3*, 327–349.

Williams, T. P., Webbers, J. P., Giordano, L., & Henderson, R. P. (1998). Distribution of photon absorption rates across the rat retina. *Journal of Physiology*, *508*, 515–522.

Wu, T. H., Ting, T. D., Okajima, T. I., Pepperberg, D. R., Ho, Y. K., Ripps, H., & Naash, M. I. (1998). Opsin localization and rhodopsin photochemistry in a transgenic mouse model of retinitis pigmentosa. *Neuroscience*, *87*, 709–717.

Xu, X., & Karwoski, C. J. (1994). Current source density analysis of retinal field potentials. II. Pharmacological analysis of the b-wave and M-wave. *Journal of Neurophysiology*, *72*, 96–105.

Young, R. W. (1984). Cell death during differentiation of the retina in the mouse. *Journal of Comparative Neurology*, *229*, 362–373.